BRL

12

AD

CONTRACT REPORT NO. 347

TRANSIENT COMBUSTION IN GRANULAR PROPELLANT BEDS. PART II: EXPERIMENTAL STUDY OF TRANSIENT COMBUSTION PROCESSES IN MOBILE GRANULAR PROPELLANT BEDS

Prepared by

The Pennsylvania State University
Department of Mechanical Engineering
University Park, PA 16802

August 1977

USA ARMAMENT RESEARCH AND DEVELOPMENT COMMAND
USA BALLISTIC RESEARCH LABORATORY
ABERDEEN PROVING GROUND, MARYLAND

Destroy this report when it is no longer needed.
Do not return it to the originator.

Secondary distribution of this report by originating or sponsoring activity is prohibited.

Additional copies of this report may be obtained from the National Technical Information Service, U.S. Department of Commerce, Springfield, Virginia 22151.

The findings in this report are not to be construed as an official Department of the Army position, unless so designated by other authorized documents.

The use of trade names or manufacturers' names in this report does not constitute indorsement of any commercial product.

UNCLASSIFIED

SECURITY CLASSIFICATION OF THIS PAGE (When Data Entered)

REPORT DOCUMENTATION PAGE

READ INSTRUCTIONS BEFORE COMPLETING FORM

1. REPORT NUMBER: BRL CONTRACT REPORT NO. 347	2. GOVT ACCESSION NO.
3. RECIPIENT'S CATALOG NUMBER	
4. TITLE (and Subtitle): Transient Combustion in Granular Propellant Beds. Part II: Experimental Study of Transient Combustion Processes in Mobile Granular Propellant Beds.	5. TYPE OF REPORT & PERIOD COVERED: Final Report, Feb. 15, 1974 - Feb. 14, 1977
	6. PERFORMING ORG. REPORT NUMBER
7. AUTHOR(s): T. R. Davis, K. K. Kuo	8. CONTRACT OR GRANT NUMBER(s): DAAG 29-74-G-0116
9. PERFORMING ORGANIZATION NAME AND ADDRESS: Department of Mechanical Engineering, The Pennsylvania State University, University Park, PA 16802	10. PROGRAM ELEMENT, PROJECT, TASK AREA & WORK UNIT NUMBERS
11. CONTROLLING OFFICE NAME AND ADDRESS: U. S. Army Research Office, Post Office Box 12211, Research Triangle Park, NC 27709	12. REPORT DATE: AUGUST 1977
	13. NUMBER OF PAGES: 88
14. MONITORING AGENCY NAME & ADDRESS (if different from Controlling Office): 1. Combustion and Prop. Br., Ballistic Research Lab., Aberdeen Proving Ground, Aberdeen, MD 21005; 2. Ballistics and Comb. Research Branch, Picatinny Arsenal, Dover, NJ 07801	15. SECURITY CLASS. (of this report): Unclassified
	15a. DECLASSIFICATION/DOWNGRADING SCHEDULE: NA

16. DISTRIBUTION STATEMENT (of this Report)

Final rept. 15 Feb 74-14 Feb 77

Approved for public release; distribution unlimited.

17. DISTRIBUTION STATEMENT (of the abstract entered in Block 20, if different from Report)

12 84p. 18 BRL 19 CR-347

18. SUPPLEMENTARY NOTES

19. KEY WORDS (Continue on reverse side if necessary and identify by block number)

Vented Chamber Experiments	Projectile Displacement Measurements
Gaseous Igniter	Traveling Pressure Front
Impact Primer Igniter	Flame Front Accelaration
Ionization Pin Measurements	Deterrent Effect

20. ABSTRACT (Continue on reverse side if necessary and identify by block number)

Catastrophic failure of propulsion and gun systems has been attributed to abnormal combustion within granular propellant charges. The effects of igniter strength, propellant type, deterrent concentration, and projectile motion on the overall transient combustion processes in granular propellant beds were studied experimentally. The results show that igniter strength significantly affects the duration of the induction period, and also the accelerative behavior of the pressure front traveling through the bed; a weaker igniter causes a more pronounced pressure front accelaration. A large igniter volume was found

DD FORM 1 JAN 73 1473 EDITION OF 1 NOV 65 IS OBSOLETE

Unclassified

SECURITY CLASSIFICATION OF THIS PAGE (When Data Entered)

401 929

20. to reduce the rate of flame spreading and pressurization processes. Combustion of slightly deterred propellants produced extremely rapid flame spreading, higher peak pressures, and higher pressurization rates than regularly deterred propellants. Propellant particle geometry was found to greatly affect the rate of total mass consumption within a propellant bed and thereby influence the peak pressures and pressure wave phenomena within the bed.

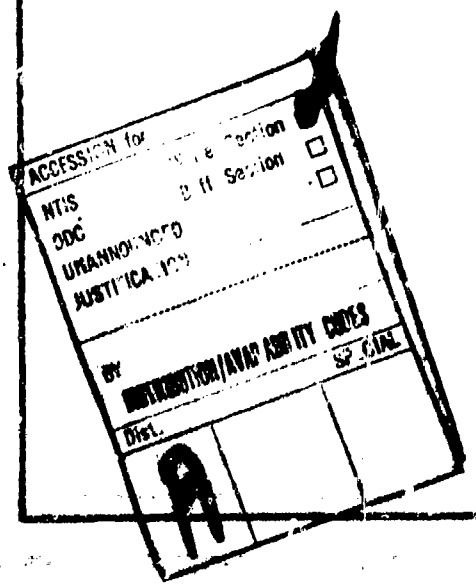

TABLE OF CONTENTS

TABLE OF CONTENTS

LIST OF FIGURES

LIST OF TABLES

CHAPTER I

INTRODUCTION

The theoretical study of transient combustion and flame spreading in granular solid propellant beds requires a parallel experimental study to provide a direct means for verification of the theoretical model. In addition, experimental results aid in the understanding of the physical process, such as the effects of primer strength, propellant type, deterrent concentration, and downstream boundary condition on the overall combustion process. The experimental study can also establish a data base which may be useful for data correlation and for providing physical input for the theoretical solution.

1.1 Motivation and Objectives

Catastrophic failure of propulsion and gun systems has been attributed to ignition transients within granular propellant charges. This research is stimulated by the need for continued investigation of the ignition and flame spreading phenomena of solid propellant combustion. The research is also partially motivated by the recent progress in the area of granular propellant studies (1-22). Besides the encouragement offered by these advancements in this field, the problem of ignition and flame spreading in porous propellant charges is obviously important in the design and analysis of propulsion systems.

Therefore, the overall research objectives of this experimental study are:

1) To verify the theoretical model which parallels this study.

2) To improve the understanding of transient combustion in order to reduce hazards and to improve the design of propulsion systems.

3) To provide the physical model and boundary conditions required in the solution of the theoretical model.

4) To evaluate the effects that a single variable (i.e., igniter strength, propellant composition, and downstream boundary) has on the transient combustion process.

The results of this study may be useful to future investigators for predicting general trends in solid propellant combustion for a wide range of combustor geometries and propellant compositions. In addition, the comparatively generalized approach to this work should be helpful in the design of future experimental test systems.

The phenomena that occur during the transient combustion event include:

a) penetration of hot ignition gases into the granular bed

b) convective heating of the propellant to ignition

c) compaction of the granular bed

d) rapid pressurization within the combustion chamber

e) propagation of the peak pressure toward the downstream end of the chamber

f) flame spreading within the propellant bed

g) rapid depressurization of the chamber following the rupture of a shear disc or motion of a projectile.

It is beyond the scope of this initial experimental effort to study these phenomena individually. Indeed, they are so interrelated

that complete segregation of each process is virtually impossible. In this respect, the purpose of this work is to describe the collective effect of these phenomena on the overall combustion process.

CHAPTER II

LITERATURE SURVEY

In this chapter a literature survey is presented on two different topics: i) a brief survey on related experimental studies in granular propellant combustion, and ii) a survey of the instrumentation currently used in combustion tests.

2.1 Survey on Related Experimental Works

The objective here is to summarize the results and conclusions of various investigations in granular propellant in order to indicate the current state-of-the art, to gain an understanding of the previously observed phenomena and also to avoid duplication of prior studies. Recent studies were made by various investigators to gain a deeper understanding of the physical phenomena in igniting and burning granular propellants.

Squire, et al (23) investigated the primer propellant interface in a constant volume venting bomb. They conclude from their experimental results that there is definitely a propagation of a flame front through the propellant bed, and that the reason for the time delay between initiation of successive gages along the chamber is explained by the finite rate of flame spreading and by the compaction effect in the bed. In addition, they show that the primer strength has a pronounced effect on the ballistic cycle. Kuo, et al (1) used Squire's results to show that gas-penetration burning of porous propellants or explosives under

strong confinement is inherently self-accelerating. Squire also studied the motion of the granular propellant particles by inserting several lead particles into the bed and observing their motion with X-ray photography. There is some doubt, however, whether these results are representative of the actual particle motion since the density of the lead particles is much greater than that of the propellant. If smaller lead particles had been enclosed in a less dense material, such that the average density of the test particles equalled the density of the actual propellant particles, then the experimental measurements would be more representative of the actual particle motion.

In the consideration of the effect of propellant type on the pressure-time-distance variations, Warlick (24) conducted several experiments on various artillery systems, using NACO propellants (the cool-burning propellant which reduces barrel erosion), and comparisons were made with the PYRO propellants. The pressure-time traces obtained at the case base showed no significant difference with propellant type. The pressure-time history at the projectile base is later found to be radically different from those recorded at the cartridge case base. The intensity of the traveling pressure front in the combustion chamber was found to be strongly dependent on primer venting, porosity distribution, and the physical-chemical characteristics of the propellant in the bed. Warlick firmly suggests that interior ballistic systems studies must include the consideration of the above effects to minimize the pressure irregularities.

Soper (22) performed experiments on ignition waves in gun chambers loaded with NACO propellants. His experimental results revealed severe

wave action during ignition: a distinct pressure wave traveled down and continued oscillating inside the combustion chamber. A strong pressure spike at the base of the projectile was recorded (the typical intensity is 2460.0 kg/cm^2). Soper's flash X-ray apparatus detected a pronounced acceleration of propellant particles ahead of the gas pressure wave. This suggests consideration of both the motion of propellants and also the intergranular forces transmitted in compaction beds are equally important.

Extensive experiments were performed by Gerri, et al (25,26) on granular propellants in a vented chamber similar to the one used in this study. Gerri primarily used WC-846 propellant grains and FA-41 primers, which were also used for a small number of experiments in this study. Photodiodes were used to measure the flame spreading in the propellant bed and for measuring the burst of the shear disc at the vented end of the chamber. Also, a microswitch was used to measure any deflection of the shear disc prior to bursting. By using several types and thicknesses of shear discs, Gerri showed that due to extremely high pressurization rates, the bursting strength of the shear disc had little effect on the pressure-time traces. There were several discrepancies in the photodiode data, however, and as a result, very little flame spreading information was obtained. The results of the pressure measurements clearly indicate a strong pressure gradient which moves along the axial length of the packed propellant bed during the combustion process. From his experimental observations, Gerri concludes that additional theoretical and experimental emphasis must be placed in the following areas: 1) Compaction of the bed

due to primer action; 2) subsequent compaction of the bed due to pressure build-up and two phase gas flow through the bed; and 3) ignition at the interface between primer and propellant.

Bernecker and Price (27-29) have studied the transition from deflagration to detonation (DDT) in porous propellant charges under confinement. To measure the flame front location during the transient event, ionization pins were glued into the walls of a thin-walled steel chamber (detonation tube) which detect the presence of ionized gases in the propellant flame. Their studies show that a convective flame front exists in burning propellant charges and that the stability of this convective front is largely determined by the properties of the propellant (i.e., the more energetic the propellant, the more stable the convective front).

Horst (30-32) has done considerable work in primer-propellant interface studies for larger caliber Navy gun systems using the bayonet-type primer. Most evident in his experimental results is the existence of extreme pressure wave phenomena and pronounced reverse pressure gradients within the casing caused by high pressure differences between the breech and projectile ends of the casing. Malfunctions of several large caliber gun systems have been attributed to these large pressure differences. In his most recent experimental work (32), Horst investigated three possible techniques to minimize and/or eliminate the extreme pressure wave phenomena: 1) elimination of void regions in the forward end of the gun casing and the addition of a radial foam spacer along the casing,

2) replacement of the standard 7-perforated grains with 19-perforated grains and 3) modification (lengthening) of the bayonet primer in an attempt to provide simultaneous ignition along the axial length of the propellant charge. Initial experimental results indicate that the first two techniques investigated were reasonably effective in reducing the reverse pressure gradient. The third technique was less successful; however, it was pointed out that by increasing the primer length further (to the entire length of the charge), axial flame spreading might be reduced significantly and the extreme reverse pressure gradients may be eliminated.

East and McClure (33) have conducted tests on two different charge assembly configurations for the 76 mm OTO MELARA weapon system and on two different charge assembly configurations for the 5"/54 weapon system. Their tests included time correlated measurements of pressure wave action via multiple pressure transducers along the propelling charge axis and projectile base, propellant grain motion via flash radiography, flame front propagation via high speed photography, projectile displacement via streak photography, and projectile acceleration via base mounted accelerometers. The radiographs revealed that the M6 grains were pulverized when they impacted with the projectile base at velocities of 800 fps. In addition, their measurements showed that for all the configurations tested, the flame front was either coincident with or lagged the pressure front throughout the propelling charge.

2.2 Instrumentation Survey

The three primary phenomena measured in this study are pressure, flame speed, and projectile displacement. To instrument a granular

propellant combustor to accurately measure these extremely rapid, transient phenomena requires electro-mechanical devices with the following characteristics:

a) high frequency response to accurately follow the transient event

b) high resonant frequency to avoid high amplitude oscillations

c) high input impedance so as not to affect the phenomena being measured

d) high durability and accuracy when exposed to extreme combustion environments

e) high output level to avoid noise problems in signal processing

f) small physical size and mass to facilitate mounting in the combustor.

In addition, a recording system is required that is capable of high frequency, multi-channel, time correlated data acquisition.

2.2.1 Pressure Measurements

A general reference (37) for pressure tranducer types and pressure sensing elements that are currently available in the commerical market is given in Appendix 1. The majority of recent experiments in solid propellant combustion (22-26,30-35) have used the KISTLER 607 piezoelectric pressure transducer. The wide acceptance of this electro-mechanical principle warranted additional study of the commercially available piezoelectric transducers in the 100,000 psi range. The results of this survey are shown in Table 1. The major difference between the various models in Table 1 is the type of signal conditioning and/or amplification required. The more expensive models include a charge amplifier which

TABLE 1

COMPARISON OF HIGH PRESSURE QUARTZ TRANSDUCERS

	KISTLER (SUNDSTRAND)		PCB		KISTLER (KRISTAL)
	607	207	108A	118A	6211
CAL. PRESS. RNG.	100,000 psi	100,000 psi	100,000 psi	80,000 psi	100,000 psi
MAX. PRESS. RNG.	----------	----------	125,000 psi	100,000 psi	114,000 psi
RESONANT FREQ.	250 KHz.	250 KHz.	300 KHz.	300 KHz.	150 KHz.
RISE TIME	1.5 μ sec.	1.5 μ sec.	2 μ sec.	2 μ sec.	2 μ sec.
SENSITIVITY	.14pc/psi	.05mv/psi	.1mv/psi	.2pc/psi	.13pc/psi
RESOLUTION	----------	----------	2 psi	2 psi	.28 psi
LINEARITY	2 %	2 %	2 %	2 %	2 %
TEMP. RNG.	-320+500°F	-65+250°F	-100+275°F	-100+400°F	-150+240°C
FLASH TEMP.	3000°F	3000°F	3000°F	4000°F	----------
MAX. SHOCK	----------	----------	20,000 g	20,000 g	15,000 g
TEMP. COEFF.	----------	----------	.03%/°F	.01%/°F	-.02%/°C
CAPACITANCE	----------	N/A	N/A	5 pc	4 pc
PRICE (APPROX)	$480.00	$510.00	$450.00	$375.00	$425.00
CHARGE AMP.	$600.00	N/A	N/A	-------	$580.00
IN-LINE AMP.	-------	N/A	N/A	$80.00	-------
TOTAL	$1080.00	$510.00	$450.00	$455.00	$1005.00

provides the capability to select an output range for a given input pressure range. This capability is not available on the models with built-in amplifiers or in-line amplifiers.

A resistive type Minihat (36) pressure transducer was developed at the Ballistic Research Laboratory especially for use in the extreme environment of interior ballistics. During the development of the gage, extensive combustion tests were made to compare the simultaneous outputs of the Minihat transducer with a Kistler 607 transducer. In the latter stages of development, the comparisons were in extremely good agreement and are presented in reference 35.

2.2.2 Flame Speed Measurements

Considerable disagreement exists among current investigators concerning the definition of the flame front. One group of investigators (27-29) defines the flame front as the arrival of the ionized gas which is known to be present in a flame. Other groups (22,25,26,33) define it as a high intensity luminous zone which travels through the propellant bed.

To measure the flame speed in granular propellant charges, Bernecker and Price (27-29) have used ionization pins. Their results have shown that the flame speed increases abruptly during the transition from deflagration to detonation. Gerri (25,26) has used photodiodes to measure flame spreading and also to measure the rupture time of the burst diaphram. Gibson and Macek (38) used a high resistance Nichrome wire embedded axially in the explosive charge to measure the flame speed in a continuous manner. The ionized flame front shorted the wire to the

grounded charge case, thereby completing the circuit. As the flame traveled through the charge, the resistance became smaller; thus a continuous measurement of the flame front was obtained. Gibson and Macek also used ionization pins to verify the Nichrome wire results and found both methods in agreement with each other.

2.2.3 Projectile Displacement Measurements

For the investigator in interior ballistics, the motion of a projectile at the downstream boundary of a propellant charge represents a transient increase in volume for the combustion process. As a result, the precise location of the projectile before leaving the gun barrel is extremely important.

Squire (23) used a microwave interferometer to measure the projectile displacement within an M16 rifle. The microwave interferometer is essentially a very high frequency (GHz) transmitter/receiver. A sine wave is propagated down the barrel of the weapon and the reflected radiation from the nose of the projectile undergoes a doppler shift as the projectile moves forward. The resulting output is a frequency varying sine wave which can be directly related to the velocity of the projectile.

Stansbury and Comer (39) have also used the microwave interferometer in their studies with liquid propellant combustion. Due to the inherent noise in the doppler signal, they have developed "smoothing" and filtering techniques to minimize errors in differentiated signals.

CHAPTER III

EXPERIMENTAL SET-UP

3.1 General Design Considerations

The transient combustion process of granular solid propellant is an extremely rapid event involving pressurization rates which exceed 14 million atm per second. Pressurization rates of this order of magnitude may create extremely hazardous experimental conditions. In this respect, the primary consideration in the design of the combustor was safety. Since each data instrument mounted in the walls of the combustor weakens the strength of the chamber, the number, size, and type of each data probe was carefully considered to maximize safety, yet still obtain meaningful data.

In addition to safety, the response time of the data probes is extremely important. Transient events of the order mentioned above require data resolution to the order of just a few microseconds.

Having defined the major considerations in the combustor design and instrumentation, it is the purpose of this chapter to present the assembled test rig and then to describe each component in detail.

A schematic drawing of the current experimental test rig is shown in Fig. 1. The main components are 1) the igniter chamber which houses the primer, 2) the main combustion chamber which contains granular propellants, and 3) the projectile chamber. During the course of these experiments, four basic combustor assembly configurations were used:

a) gaseous ignition system with shear disc and shear disc retainer;

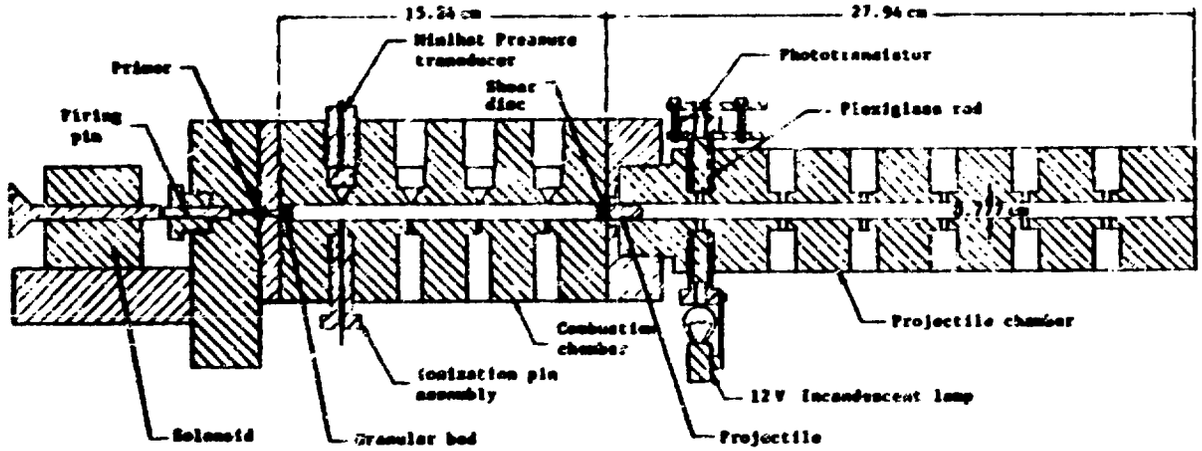

Figure 1 Schematic Drawing of the Experimental Test Rig

b) gaseous ignition system with projectile and projectile chamber;

c) impact primer ignition system with shear disc and shear disc retainer; and

d) impact primer ignition system with projectile and projectile chamber.

A schematic drawing of the configuration using the gaseous ignition system with shear disc and shear disc retainer is shown in Fig. 2.

3.2 The Combustion Chamber

The thick-walled combustion chamber is fabricated from "Elastoff 44" steel, and is designed to contain rapid pressure transients in excess of 15,000 atm. The chamber has an outside diameter of 8.89 cm, and a smooth center bore of 0.777 cm. The length of the chamber is 15.24 cm. Each end of the chamber contains an alignment ring to ensure a perfect concentric alignment of adjoining sections of the combustor (igniter and projectile chamber). A 5/8 inch diameter O-ring (1/8 inch cross-sectional diameter) of type Buna N rubber provides a pressure seal at each end of the chamber. The combustion chamber houses four pressure transducers and four ionization probes which are evenly distributed and spirally located along the length of the chamber. Each ionization pin is located diametrically opposite to a pressure transducer. The spiral placement of the pressure transducers and ionization pins is intended to maximize combustion chamber strength and to verify the theory that the combustion process is essentially one-dimensional along the axial length of the granular propellant bed.

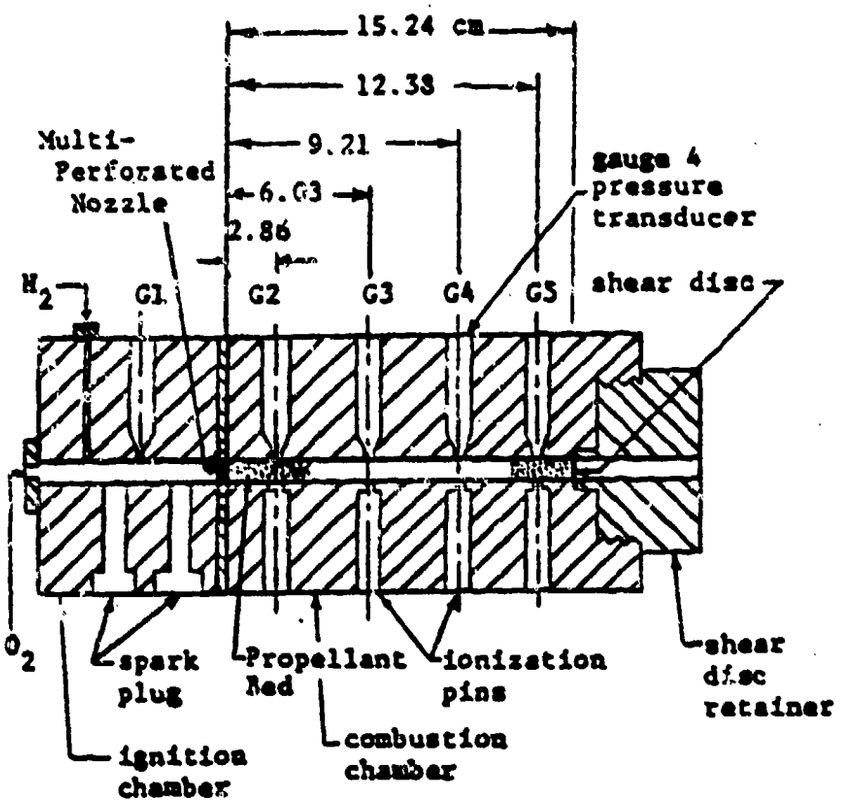

Figure 2 Schematic Drawing of the Combustor with the Gaseous Ignition System, Shear Disc, and Shear Disc Retainer

3.3 Gaseous Ignition System

Two ignition systems have been developed for igniting the granular propellant bed: a gaseous H_2-O_2 ignition system and an impact ignition system. The gaseous igniter, which was used primarily during the earlier phases of testing, is shown in Fig. 3. This type of ignition provides the capability to readily vary igniter strength and duration. Igniter mass flow rate is determined by the choked flow equation using the measured ignition chamber pressure and the adiabatic flame temperature for the mixture. The igniter strength is controlled by regulating the oxidizer-fuel ratio and the amount of reactants in the chamber. Hydrogen and Oxygen were chosen as the reactants because of their easy ignitability by sparks, and wide flammability limits. The gaseous reactants are mixed in the ignition chamber by injecting hydrogen tangentially into the oxygen stream to achieve good turbulent mixing within a short distance. Two spark plugs are recessed from the flow stream and recirculation eddies in the recessed cavities act as flame holders which stabilize the flame in the high velocity gas stream.

The ignition and combustion chambers are separated by a multi-perforated convergent nozzle, shown in Fig. 4. The nozzle is covered and tightly sealed by tape on the upstream side to prevent unburned reactant gases from entering the propellant bed before ignition. The design of the nozzle is intended specifically to provide uniform heating of the granular propellant, to achieve a one-dimensional flow condition, and also to provide a one-dimensional compaction of the bed.

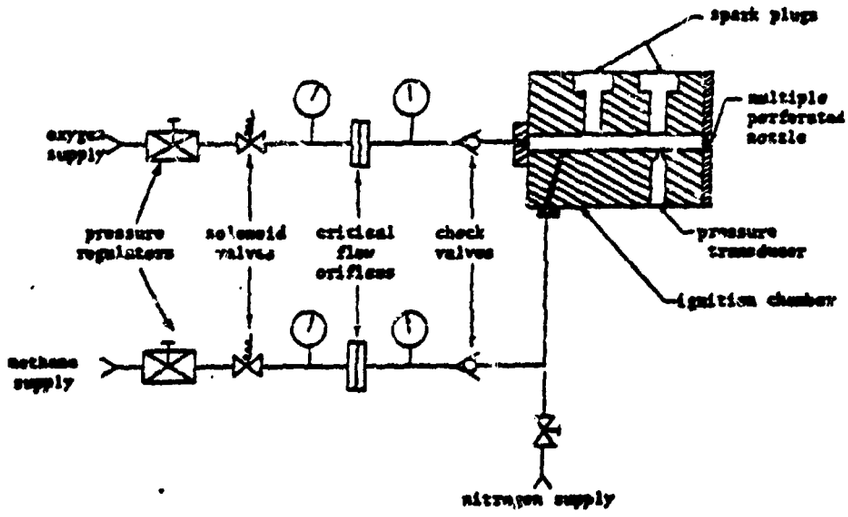

Figure 3 Schematic Drawing of the Gaseous Ignition System

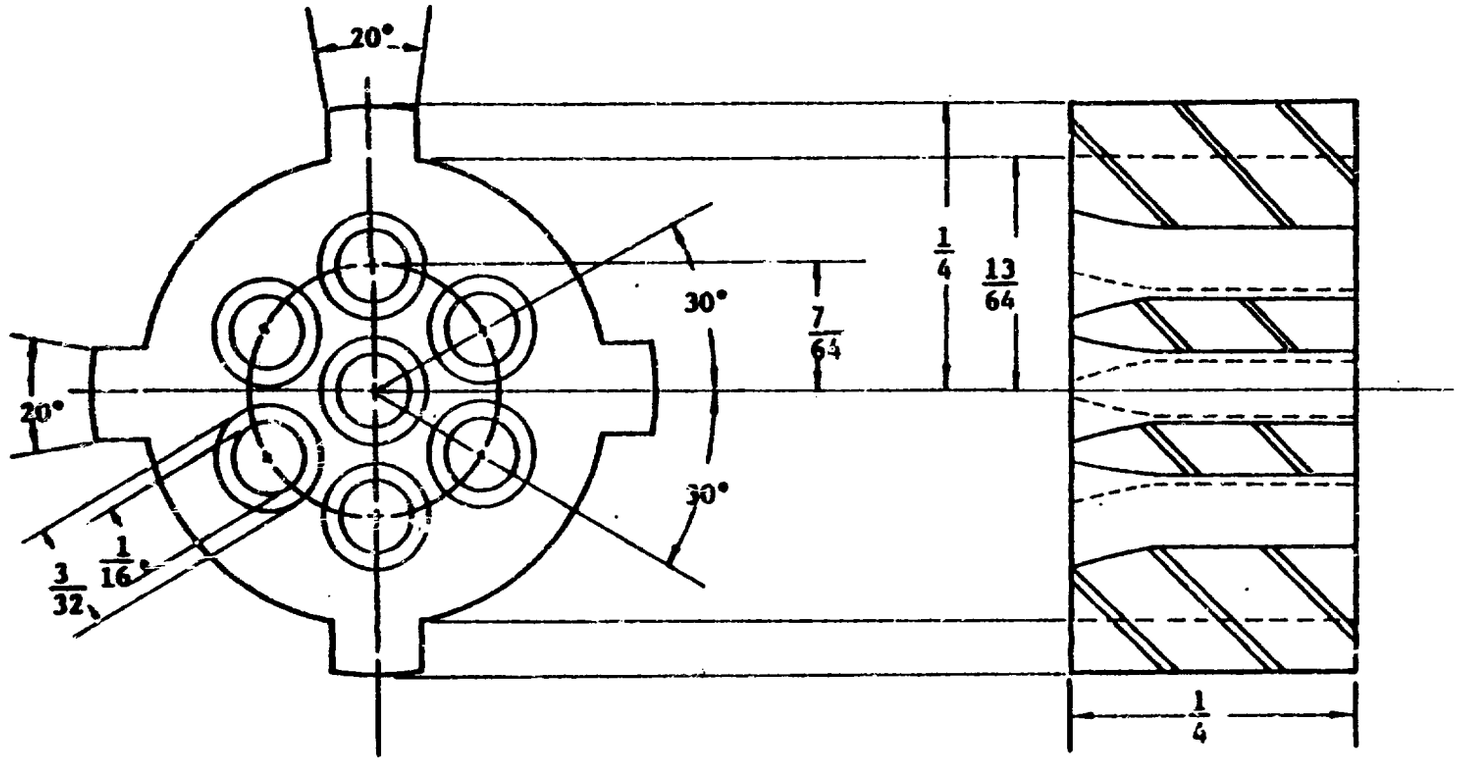

Figure 4 Schematic Drawing of the Multi-Perforated Convergent Nozzle

3.4 Impact Primer Ignition System

The impact ignition system (more commonly called a primer), which has been used in the later phase of the experimental study, is shown in Fig. 5. This igniter provides an extremely short induction period compared to that of the gaseous igniter. The smaller volume of the impact primer results in significantly less back flow than the gaseous system which in turn produces higher peak pressures and corresponding higher flame spreading rates in the granular propellant bed.

The strength of the impact primer cannot be varied as readily as the gaseous system; however, various sizes of primers of identical composition are available. This permits a limited capability to vary the strength of impact igniters.

The impact ignition system consists of a 120 VAC solenoid, a firing pin, and a small primer cartridge which contains the explosive charge. The density and mass fraction of each constituent in the primers used in this study are given in Table 2. Ignition is achieved in the following sequence: A series of ignition switches are activated which supply 120 VAC to the igniter solenoid. The magnetic field established in the solenoid causes the solenoid armature to more forward and strike the firing pin. When the armature strikes the pin, a 2 VDC signal is grounded and the resultant DC pulse is recorded as a reference time for the combustion event. Simultaneously, the firing pin strikes the primer cartridge, causing the primer blast, which is subsequently discharged into the granular propellant bed.

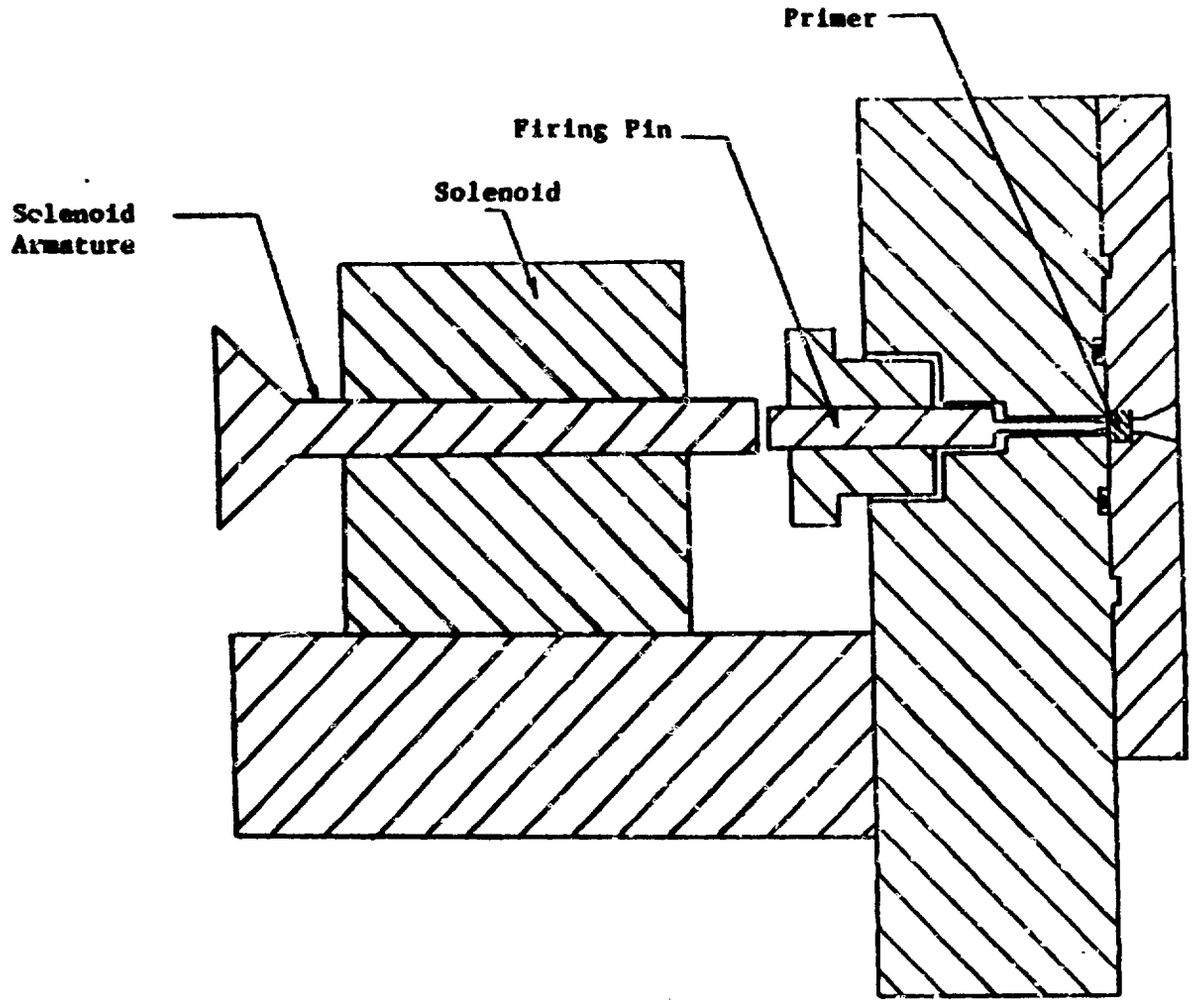

Figure 5 Schematic Drawing of the Impact Primer Ignition System

TABLE 2

PHYSICAL AND COMPOSITIONAL DATA OF FA-34
AND FA-41 PRIMERS(40)

INGREDIENT	% BY WEIGHT	DENSITY(g/cc)
PETN	5.0 ± 1	1.77
Lead Styphnate	37.0 ± 5	3.02
Tetracene	4.0 ± 1	1.05
Aluminum Powder	7.0 ± 1	2.70
Antimony Sulfide	15.0 ± 2	4.12
Barium Nitrate	32.0 ± 5	3.24

Average Density of the Mixture = 3.092 g/cc

Weight of FA-34 primer = 0.400 grains

Weight of FA-41 primer = 0.300 grains

3.5 Projectile Chamber

The last section of the test rig is the projectile chamber which is a smooth-bore, 30 caliber, thick-walled gun barrel. To observe the transient location of the projectile, a light source-sensor system has been developed. This system is currently capable of providing six distinct position-time points for the displacement of the projectile during the combustion process. Each channel of the light system works in the following manner: Light generated from a 12 volt lamp travels through a 2.5 cm plexiglass rod mounted in the wall of the chamber. It travels across the 30 caliber bore and through another 2.5 cm plexiglass rod which is mounted diametrically opposite to the first rod. The light is then received by a phototransistor. The six beams of the light system are spaced 3.81 cm apart along the length of the projectile chamber.

In order to permit a pressure build-up in the combustion chamber prior to motion of the projectile, and to simulate the cartridge friction before shot start, the base of the projectile is glued to a 1.27 cm diameter stainless steel shear disc. The 0.81 mm thick disc is "sandwiched" between the projectile chamber and the combustion chamber. When the pressure in the combustion chamber has reached a critical value (2,072 atm), the shear disc ruptures and the projectile starts to move. The projectile represents a moving downstream boundary and provides a transient increase in volume for the combustion process. However, during the initial phase of the study, the projectile and projectile chamber were replaced by a shear disc and shear disc retainer (Fig. 2). This configuration represents a fixed downstream boundary until the disc

ruptures, at which time the combustion event is terminated with a rapid depressurization of the combustion chamber. The shear disc used in the fixed-boundary study was identical to that used with the projectile configuration and the shear disc retainer was merely a shortened version (length = 5 cm) of the projectile chamber in order to provide the same shearing effect at the downstream boundary.

3.6 Instrumentation

As shown in Fig. 1, the combustor is instrumented with four pressure transducers, four ionization pins, and six photo optic sensors. In addition, a simple DC circuit connected to the solenoid armature of the primer indicates the time the firing pin starts in motion.

3.6.1 Pressure Transducers

The Minihat pressure transducers (36) are resistance-type transducers with a pressure range of 100,000 psi and a sensitivity of 20,000 psi/Ω, nominal. The gauges are periodically calibrated at the Ballistics Research Laboratories to a static pressure of 50,000 psi. The resistive element of the gauge represents a single arm of a Wheatstone bridge, as shown in Fig. 6. An electrical calibration is provided by a shunt resistor which parallels a 40 Ω resistance in the same bridge arm as the resistive element of the gauge. When the shunting switch is closed, the parallel combination produces a step function output equivalent in magnitude to a pressure signal of 50,000 psi.

3.6.2 Ionization Pins

The location of the flame front in the propellant bed during the transient event is measured by four ionization pins evenly spaced and

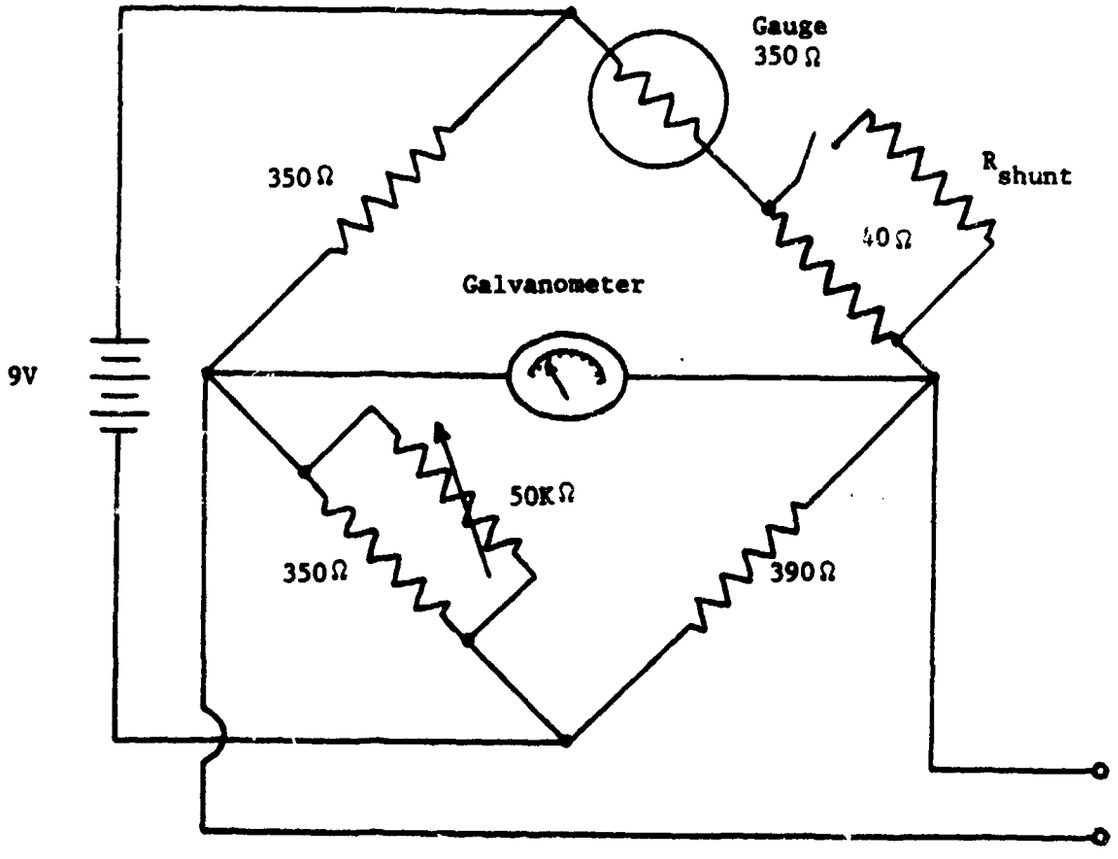

Figure 6 Schematic Diagram of the Minibat Bridge Circuit

spirally located along the length of the combustion chamber. Physically, the ionization pin is a small (.032 in O.D.) coaxial tube with a dielectric material separating the inner and outer conductors. The pin is mounted in the wall of the chamber in such a manner that the tip of the pin is flush with the inside wall of the chamber. Electrically, the pin represents a switch in a simple RC circuit as shown in Fig. 7. When the switch closes, the capacitor discharges and a single pulse is developed across the output resistor. During the combustion process, as the flame front passes an ionization pin, the ionized gases in the flame provide a path for current flow from the inner to outer conductor of the pin, thereby closing the switch of the ionization pin circuit and producing a single pulse output.

3.6.3 Projectile Displacement Measurement

As previously described in Section 3.5, the location of the projectile is measured by a light source -- photo sensor system. Each phototransistor is the initial phase of a timing generator circuit. When light is received by a phototransistor, no output is generated from the circuit. However, when the projectile moves down the projectile chamber, it interrupts the light beam to each phototransistor and a single pulse is generated by each of the six circuits. The timing generator circuits have been designed to generate one single pulse and then become disabled. This design is required to prevent "false signals" when unburned propellant particles flowing behind the projectile interrupt the light beams to the phototransistors. In order to reduce the number of tape recorder channels required for the timing generator circuits, the six output

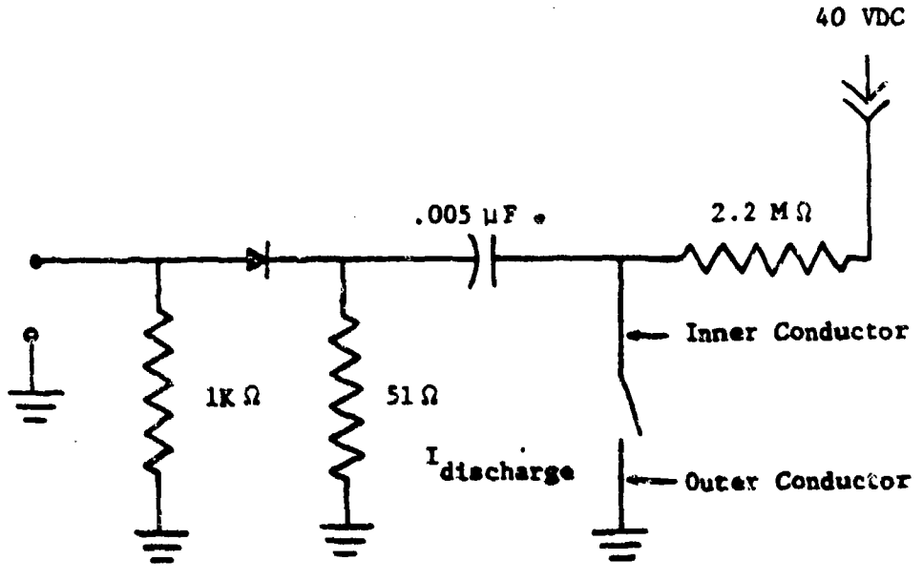

Figure 7 Schematic Diagram of a Single Ionization Pin Circuit

circuits are combined into three data channels. To accomplish this and still maintain adequate resolution of the timing pulses, channel 1 is combined with channel 2, channel 3 with channel 4, and channel 5 with channel 6.

3.7 Data Acquisition System

A block diagram of the data acquisition system is shown in Fig. 8. A wiring diagram of the system is given in Appendix 3. Currently, 15 data signals are generated for each test firing (4 pressure transducers, 4 ionization pins, 6 phototransistor signals, and 1 trigger pulse). The bridge circuits for the pressure transducers are powered by a 6 channel Acopian model 2115 9 volt DC regulated power supply. The output of each bridge is amplified by a six-channel 50 db wide band preamplifier which was manufactured by the Electronic Services Department of The Pennsylvania State University. Following amplification, the pressure data are recorded on a high speed magnetic tape recorder.

The ionization pins receive power from four 40 volt Ever ready power cells. The output of the ionization pin circuits require no amplification or signal processing and are recorded directly onto the tape recorder.

The six channel timing generator used in measuring the projectile displacement is powered by a single channel of the power supply used with the bridge circuits. As described in the previous section, the six signals are combined into three and then recorded directly onto the tape. The trigger pulse also requires no amplification and is recorded directly onto the tape.

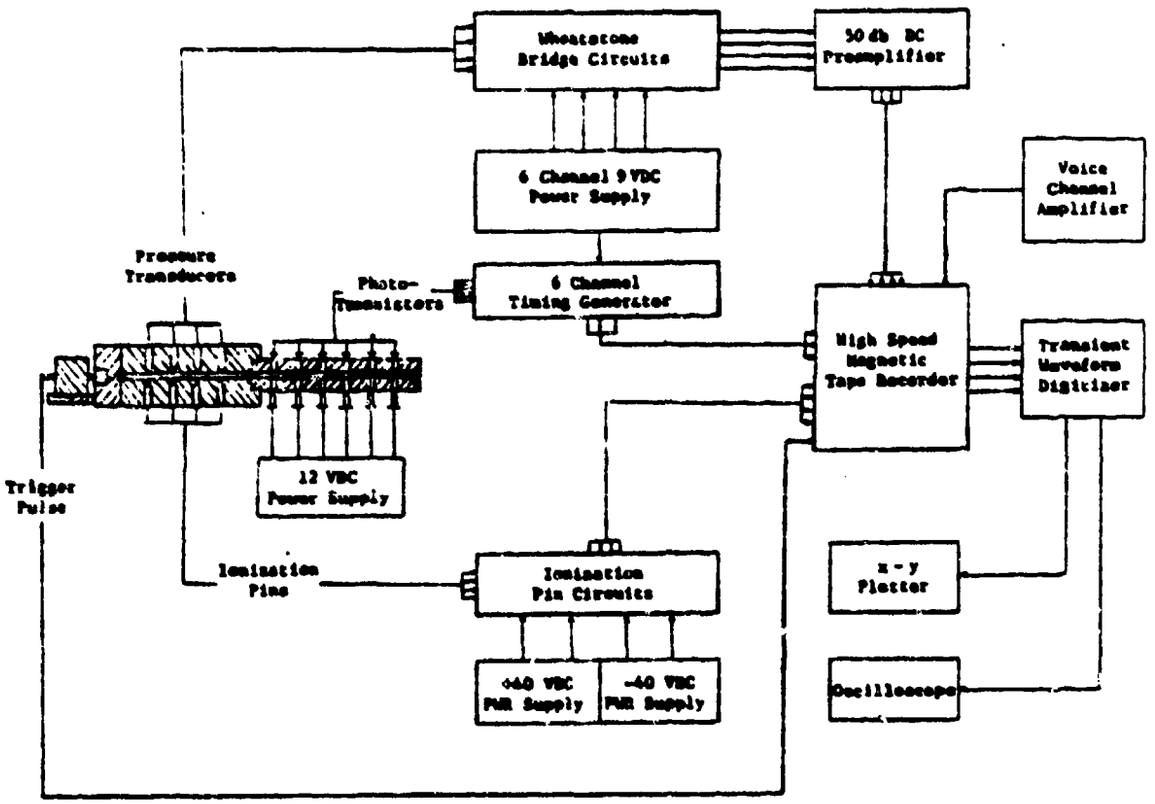

Figure 8 Block Diagram of the Data Aquisition System

The high speed magnetic tape recorder is a Hewlett-Packard model 3924 B with a simultaneous 14 channel record/reproduce capability. Seven channels record in the F.M. mode with a bandwidth of DC-20 KHz and a frequency response of +0, -1 dB. The other seven channels record in the Direct mode with a bandwidth of 300 Hz to 250 KHz and a frequency response of +0, -1 dB. In addition, an edge track is available to record the output of the voice channel amplifier.

When the tape recorder is operated in the reproduce mode, its output is recorded by a Biomation 1015 Transient Waveform Digitizer. The Biomation unit provides 4 channel data storage, 1024 bit memory per channel, and is capable of a maximum real-time resolution of 10 μ seconds. When operating in the maximum resolution mode, the time axis output of the Biomation is expanded by a factor of 10,000. The output of the Biomation is used to drive the horizontal and vertical deflection of an x-y plotter to obtain a hard copy of the 15 time-correlated data signals.

CHAPTER IV

EXPERIMENTAL RESULTS OF GRANULAR BED COMBUSTION

It is the purpose of this chapter firstly to present the experimental data obtained for a particular set of conditions which will be called the Reference Case. Using this as a basis, a qualitative explanation of the physical processes that occur during the rapid combustion event will be given. Secondly, data will be presented for which a single variable has been changed from the reference case and a direct comparison will be made in order to study the effects of primer strength, propellant type, and boundary conditions. In addition, the data are used for the verification of the theoretical model.

4.1 The Reference Case

For convenience of comparison, the reference case has been selected as a test firing with the following conditions:

a) WC-870 ball propellant (properties are listed in Table 3);

b) 7.00 gm loading weight in a 30 caliber chamber, 15.24 cm long;

c) FA-34 impact primer (constituents of the primer are listed in Table 2); and

d) 0.81 mm stainless steel shear disc at the downstream boundary.

A schematic diagram of the experimental apparatus for the reference case is shown in Fig. 9.

4.1.1 Experimental Data

The results for a typical test firing for the reference case are shown in Fig. 10; the curves are shifted vertically for clarity. The

TABLE 3

PHYSICAL, COMPOSITIONAL AND THERMO-CHEMICAL DATA OF WC 870 PROPELLANT*

Particle Shape = Spherical

Granulation
Max Particle Diameter = 0.0965 cm
Min Particle Diameter = 0.0686 cm

Gravimetric Density = 0.960 gm/cc

% Nitroglycerin = 10.0

% Nominal Nitrogen
Content of Nitrocellulose = 13.15

% Deterrent Coating = 5.20

Heat of Explosion = 870 cal/gm

Flame Temperature = 2831 °K

*This WC 870 Propellant was manufactured by Olin Corporation, Winchester Group

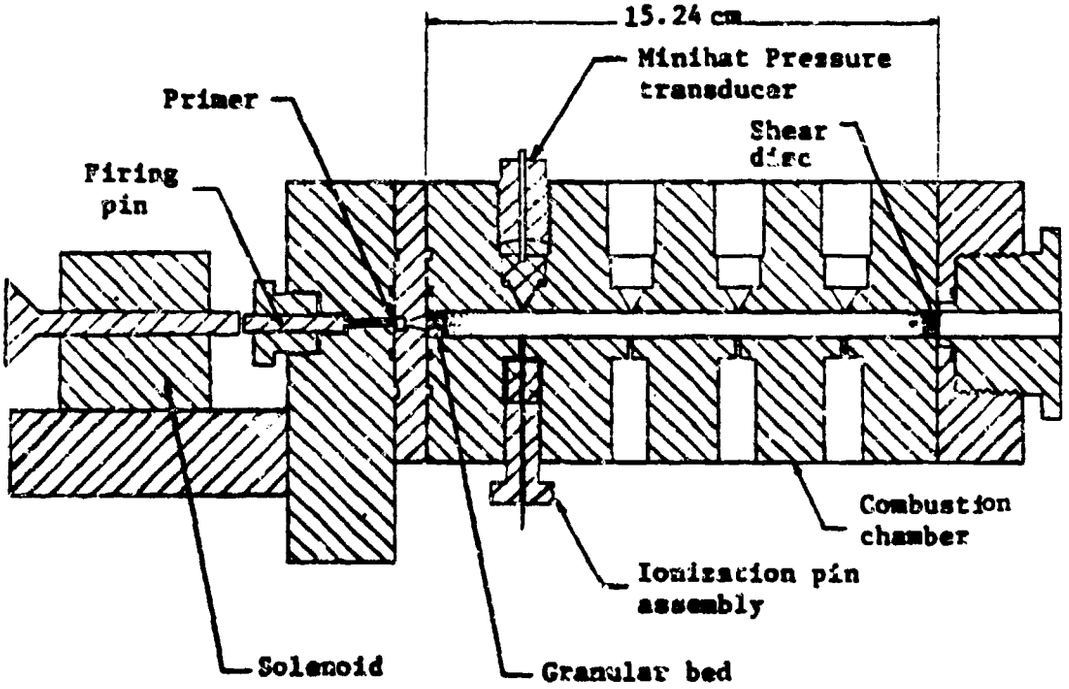

Figure 9 Schematic Drawing of the Combustor with Impact Primer, Shear Disc, and Shear Disc Retainer

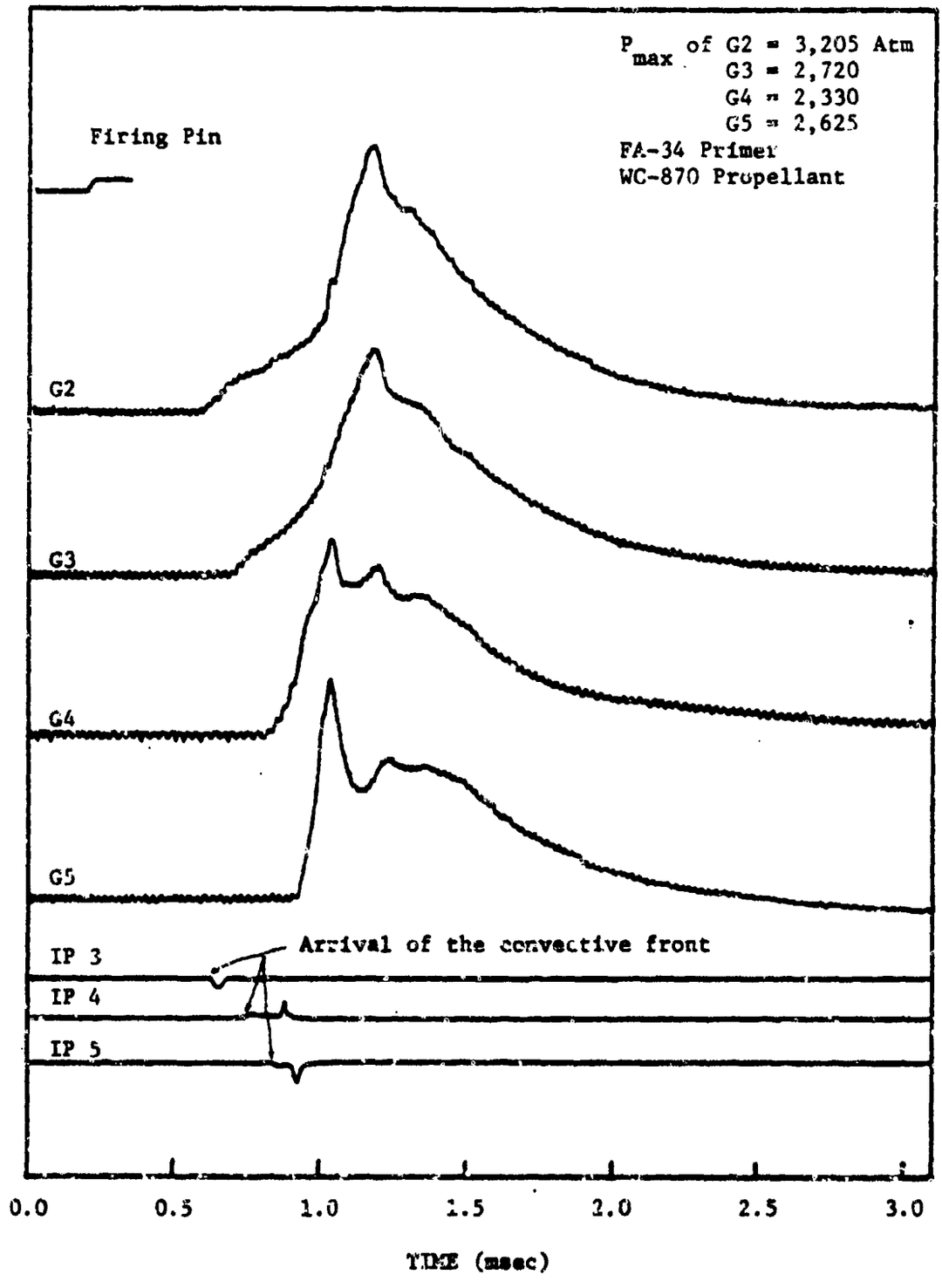

Figure 10 Typical Pressure-Time and Flame Spreading Data for the Reference Case (DAP test No. 87)

relative positions of the pressure gauges are given in Fig. 2; note that gauge 1 (G1) is used only with the gaseous igniter. Only three ionization pin traces are shown here because IP 2 is discharged by igniter gases and occurs simultaneously with the firing pin pulse. Since it does not give useful information about flame spreading, IP 2 was not used for most of the test firings. Note also that IP 3,4,5 are located directly opposite to gauges 3, 4, and 5, respectively.

From Fig. 10, several significant phenomena can be immediately seen:

a) the first discernible pressure rise for each pressure gauge occurs consecutively for G2 to G5, indicating the existence of a pressure wave traveling along the length of the chamber;

b) the pressurization rate increases consecutively for downstream positions;

c) the downstream gauges (G4, G5) indicate a second pressure peak, whereas the upstream gauges (G2, G3) show only a single peak;

d) the first discernible voltage on each IP trace occurs slightly before the first discernible pressure rise at each position;

e) before the shear disc ruptures, the pressure at the last gauge (G5) overtakes the pressures at the upstream locations; and

f) all gauges depressurize at approximately the same rate.

4.1.2 Explanation of the Physical Process

These observations can be explained in the following manner. The time delay between the first discernible pressure rise of each gauge is due to the finite time period required for the penetration of the hot product gases into the interstitial voids, resulting in a finite rate of flame spreading through the granular bed. The increased pressurization rate for downstream positions can be understood by considering the

sequence of pressure wave development through the granular bed. After the primer discharges into the combustion chamber, the upstream propellant grains ignite and begin to gasify, establishing a relatively weak pressure wave which travels in the downstream direction. Progressively, additional propellant begin to gasify, thus creating a higher pressure behind the pressure front. As the pressure level increases, the burning rate, and thus the rate of gasification, increases, which in turn causes even higher pressures. As the process continues, the pressure and the rate of gasification and pressurization continue to progressively increase, creating higher pressures and thus higher gasification rates. This "snowball" effect during the combustion of granular solid propellant is what causes an extreme pressure gradient at the pressure wave front. From the pressure-time traces and flame spreading data of Fig. 10, it is conceivable that for a much longer combustion chamber under strong confinement, the pressurization rate would continue to increase until eventually DDT occurred. Other investigators (27-29) have shown that the diameter of a porous propellant charge also affects the rapid combustion process. Therefore, an important parameter in gun system design is the length-to-diameter ratio for end burning propellant charges.

The second pressure peak experienced by the downstream gauges (G4, G5) is the result of the rupture of the shear disc. Upon rupturing, the subsequent forward motion of the shear disc establishes a rarefaction wave which travels backward through the chamber. This expansion wave causes an abrupt dip in pressure at the G5 and G4 locations, while the upstream gauges, G2 and G3, continue to show a smooth pressurization

since they are unaffected by the rarefaction wave until a later time. G2 and G3 indicate an almost simultaneous peak pressure at the arrival of the rarefaction wave since, by this time, the porosity in the upstream region has increased substantially due to particle motion and burning. The second pressure peaks indicated by G4 and G5 are caused by compression waves which are generated in the region near the igniter and by the motion of burning particles toward the downstream portion of the bed.

The theory that a convective front precedes the pressure front through the propellant bed is further supported by the ionization pin data which indicate that the ionized product gases (or flame) arrive at downstream positions slightly ahead of the pressure front traveling through the bed. In Fig. 10, IP 4 and IP 5 consistently indicate a second pulse which occurs after the arrival of the steep pressure front. It is believed that this second pulse is caused when the pin is physically shorted to the wall of the chamber due to the extreme impact of the steep pressure wave. IP 3 consistently indicates a single pulse since the pressure front is still relatively weak and does not crush or destroy the ionization pin as it does for downstream positions. In Chapter 2, it was mentioned that previous investigators have used ionization pins to measure the speed of flame front propagation through a porous propellant charge. The results of the current study, however, prove inconclusive as to whether the ionization front is actually the ignition front of the particles. These results suggest that the ionization pins might just as well indicate the time that the combustion product gases arrive at a given location, and there is no experimental evidence to date relating

the flame front to the product gases in granular propellant combustion. Therefore, the term "convective front" will be used to describe some convective mechanism -- either hot product gases, or ignition front, or both -- which slightly precedes the pressure front through the porous propellant charge. Using this definition, then, the ionization pin data in Fig. 10 show that the convective front accelerates slightly as it travels downstream through the bed.

Before the shear disc ruptures, the pressure at the last gauge position, G5, overtakes the pressure at the upstream. This phenomenon occurs consistently in every test firing and is the result of the extreme pressure gradient due to the snowball effect described above. In general, the rupture of the shear disc may be caused by intergranular stresses which are transmitted through the propellant bed or by the arrival of the pressure front or a combination of these two mechanisms. The exact cause of the shear disc rupture is still unknown; however for small arms systems, it is believed that granular stress at the shear disc is small due to high wall friction, and therefore rupture of the disc is caused mainly by the arrival of the pressure wave.

After the rupture of the shear disc, a significant quantity of unburned propellant is discharged from the downstream portion of the bed, resulting in a large void within the chamber. At this time, all spatial dependence becomes negligible as shown by the uniform depressurization of all gauges in the chamber. Downstream gauges have a slightly more rapid depressurization due mainly to their proximity to the vented end of the combustion chamber.

4.2 Effects of Igniter, Propellant Type, and Downstream Boundary

Having defined the reference case for this study and having briefly explained the most significant phenomena, the purpose of this section is to alter a single variable of the reference case and then observe any notable changes in the test results. The various cases tested are listed below:

Case 1) Gaseous H_2-O_2 igniter to replace FA-34 primer.

Case 2) FA-41 primer to replace FA-34 primer.

Case 3) WC-846 propellant to replace WC-870 propellant.

Case 4) Undeterred WC-846 propellant to replace WC-870 propellant.

Case 5) Projectile to replace the shear disc.

4.2.1 Effect of Igniter Strength

The primer-propellant interface is one of the most important characteristics in the design and modelling of modern gun systems. Previous investigations have indicated that the initial strength of the ignition source can greatly affect the peak pressures and pressurization rates in an end-burning porous propellant charge long after the igniter has been exhausted. Three types of ignition sources have been used in this study: a gaseous H_2-O_2 igniter and two solid explosive impact primers.

4.2.1.1 Case 1: Gaseous H_2-O_2 Igniter

The pressure time results of a typical test firing using the gaseous H_2-O_2 igniter are given in Fig. 11 (refer to Figure 2 for experimental test set up). The general shape of the p-t traces is quite similar to that of the reference case. The pressurization process down-

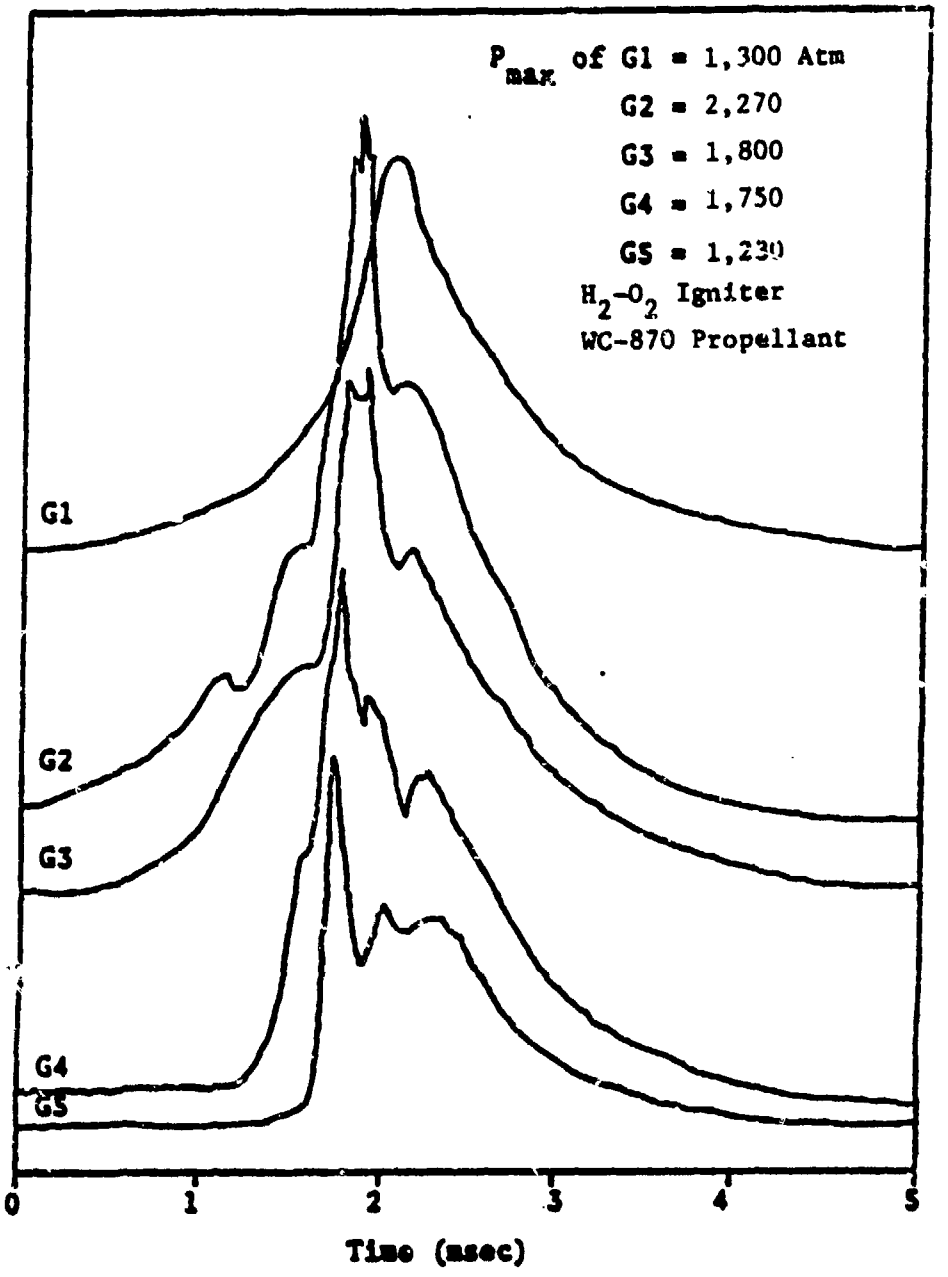

Figure 11 Typical Pressure-Time Traces for the Case 1 Assembly Configuration (Traces are offset vertically for clarity)

stream increases faster and eventually overtakes the upstream pressure traces. In addition, the data show that the rate of pressurization invariably increases in the downstream direction. In Fig. 11, the pressure transducer, G1, was positioned in the ignition chamber, and because of a choked back flow condition at the nozzle, it lags the rise in pressure at the G2 position. As in the reference case, an upstream gauge (such as G2) senses the pressurization much sooner than the gauges at downstream positions, and the rate of pressurization is significantly higher for the downstream gauges. Similarly, the pressure peak for G5 occurs slightly ahead of G2 because of the rarefaction wave phenomenon described in Section 4.1.2. The most significant differences between this case and the reference case are the magnitude of the peak pressures and the total time for the combustion event.

The reduced pressures for the Case 1 configuration are most probably explained by the larger volume of the gaseous system which results in a reverse flow of product gases through the multi-convergent nozzle into the ignition chamber. This increased volume (about 50% of the volume of the combustion chamber) is not available with the impact primer system. In addition, the reverse flow of hot product gases results in a decrease in the amount of product gases available to heat the unburned (downstream) propellant to ignition. As a result, the convective mechanism described in Section 4.1.2 is significantly weakened and consequently the combustion event requires approximately twice the time as the reference case.

As previously discussed, one of the primary objectives of this experimental study is to provide a direct means of comparison for the theoretical model. Figures 12-15 show a comparison of the pressure-time history for four positions along the bed for Case 1. The experimental data are represented as a composite of six firings (shaded areas) to show the band or range in which the data fall. The theoretical predictions are represented as a single dark line and are calculated only prior to the rupture of the shear disc. An inspection of Figs. 12-15 shows the general reproducibility of the Case 1 test firings and the relatively good agreement between theory and experiment with pressure magnitude, pressure slope and pressure rise times at each gauge location. Figure 12 shows that a major portion of the predicted pressure at G2 lies within the range of experimental firings; for the early part of the transient interval, the calculated value of pressure is lower than the experimental data. This is probably either due to the uncertainty in bed compaction by primer blast or due to the empirical correlation used for the flow resistance calculations. The resistance correlation was obtained under a no combustion condition which may result in a higher calculated bed resistance than the real test condition. A more complete comparison is given in Reference 5.

4.2.1.2 Case 2: FA-41 Primer

The chemical composition of the FA-41 impact primer is identical to that of the FA-34 primer but physically it is approximately 75% of the volume. This smaller size results in a weaker ignition source with

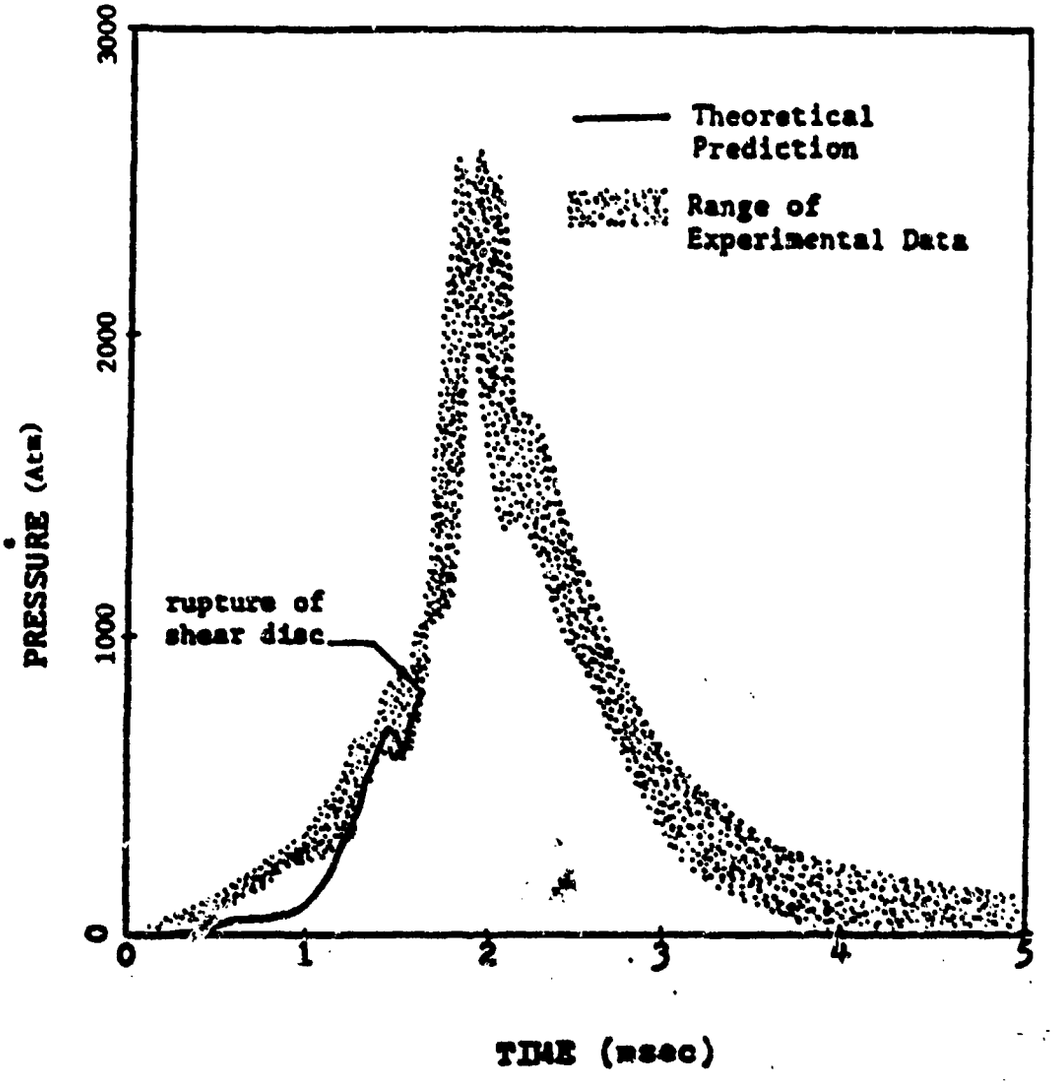

Figure 12 Comparison of the Theoretically Predicted G2 Pressure Trace with the Composite of Six Case 1 Experimental Firings

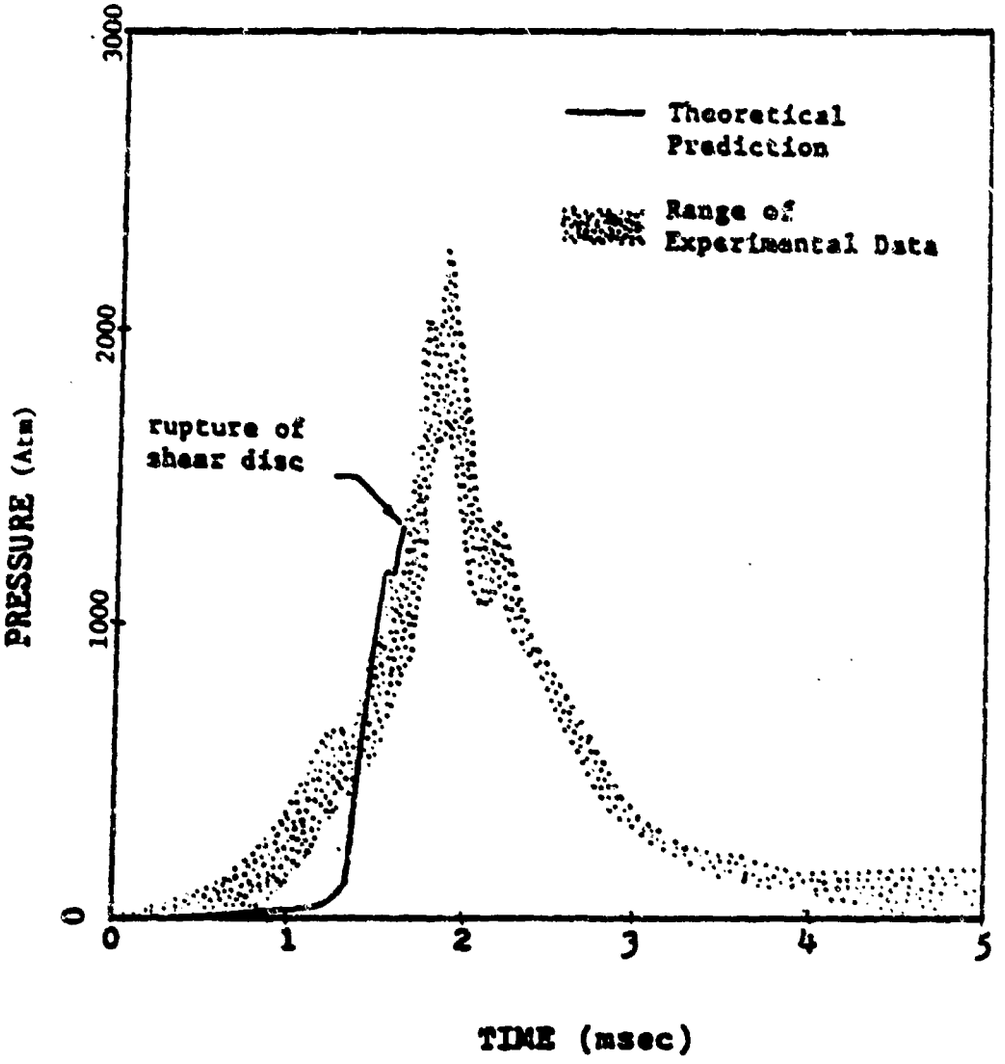

Figure 13 Comparison of the Theoretically Predicted G3 Pressure Trace with the Composite of Six Case 1 Experimental Firings

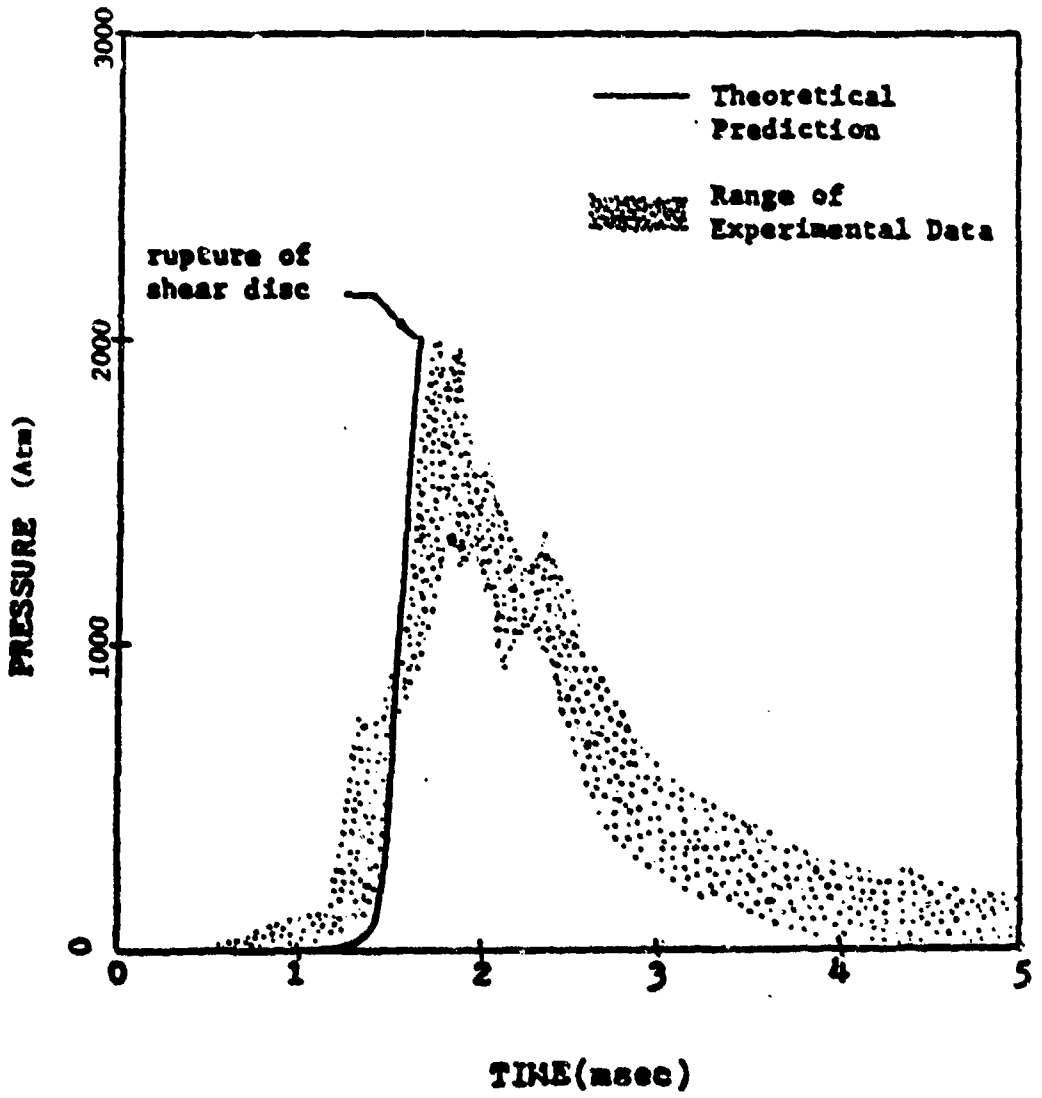

Figure 14 Comparison of the Theoretically Predicted G4 Pressure Trace with the Composite of Six Case 1 Experimental Firings

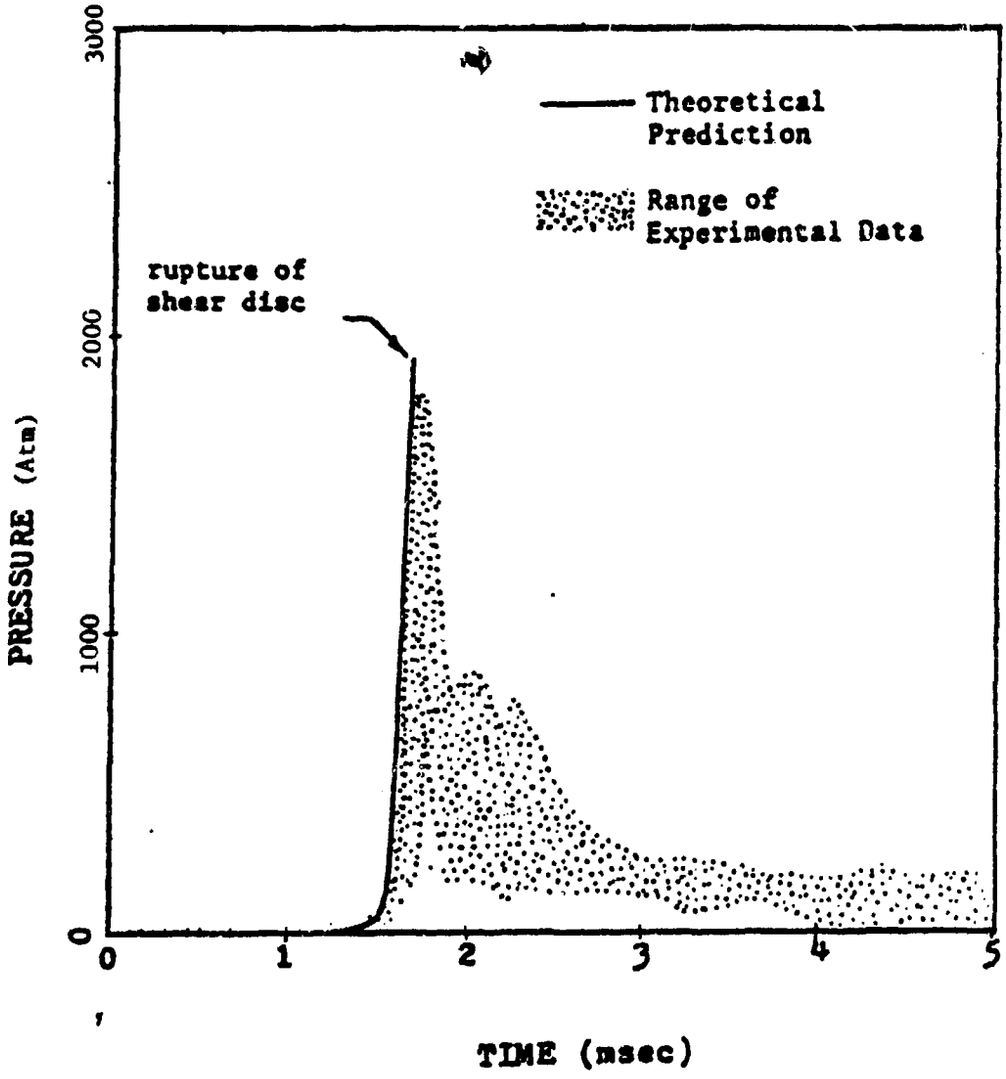

Figure 15 Comparison of the Theoretically Predicted G5 Pressure Trace with the Composite of Six Case 1 Experimental Firings

a smaller igniter mass flow rate. A typical test firing using the FA-41 primer with the WC 870 ball propellant is shown in Fig. 16. The two most significant features of this case are (1) the very slow initial burning and pressurization at the G2 location (upstream) followed by a rapid acceleration of the pressure front, and (2) the absence of sharp pressure peaks for all positions along the bed.

A comparison of the pressure-time traces of Case 2 and the reference case is given in Fig. 17. This direct comparison by starting the first discernible pressure rises at G2 from the same time clearly shows that the weaker primer produces slower burning and smaller pressure slopes than the reference case during the initial phase of the combustion event (G2). Once the granular propellant has ignited, however, the pressure front accelerates at a much faster rate until the downstream gauges (G4 and G5) exhibit the same pressure slopes as the reference case. The smaller igniter mass flow rate for the Case 2 firing results in a lower rate of convective heat transfer during the initial stages of burning. This in turn decreases the initial rate of flame spreading within the bed, resulting in a decreased spatial variation of pressure along the chamber. In addition, the weaker primer does not compact the propellant bed as much as the stronger primer of the reference case; less compaction results in more void volume in the downstream portion of the bed. Since the propellant particles are not as tightly packed, there is less flow resistance within the bed. As a result, the acceleration of the convective front becomes more pronounced.

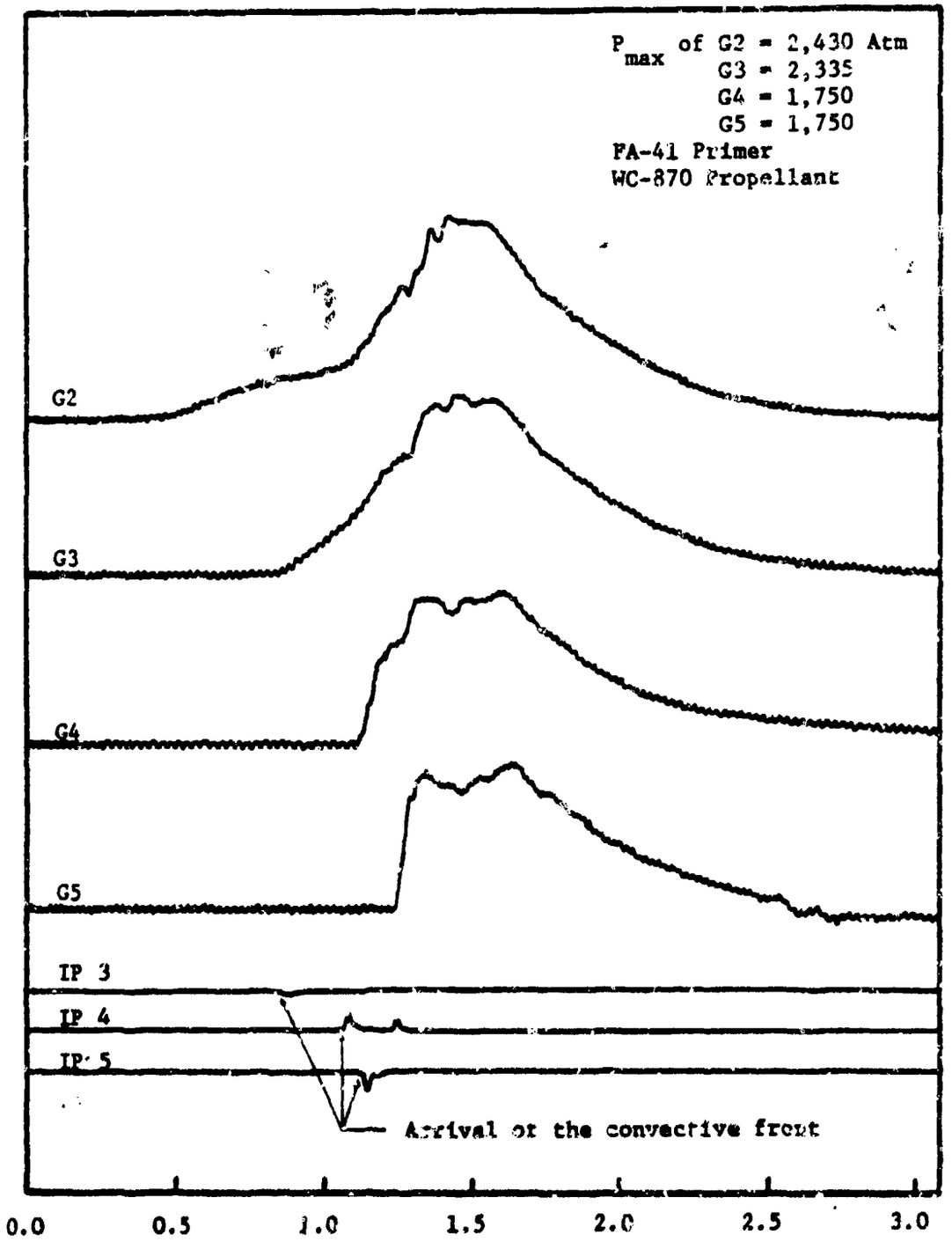

Figure 16 Typical Pressure-Time and Flame Spreading Data for a Case 2 Test Firing (DAP Test No. 88)

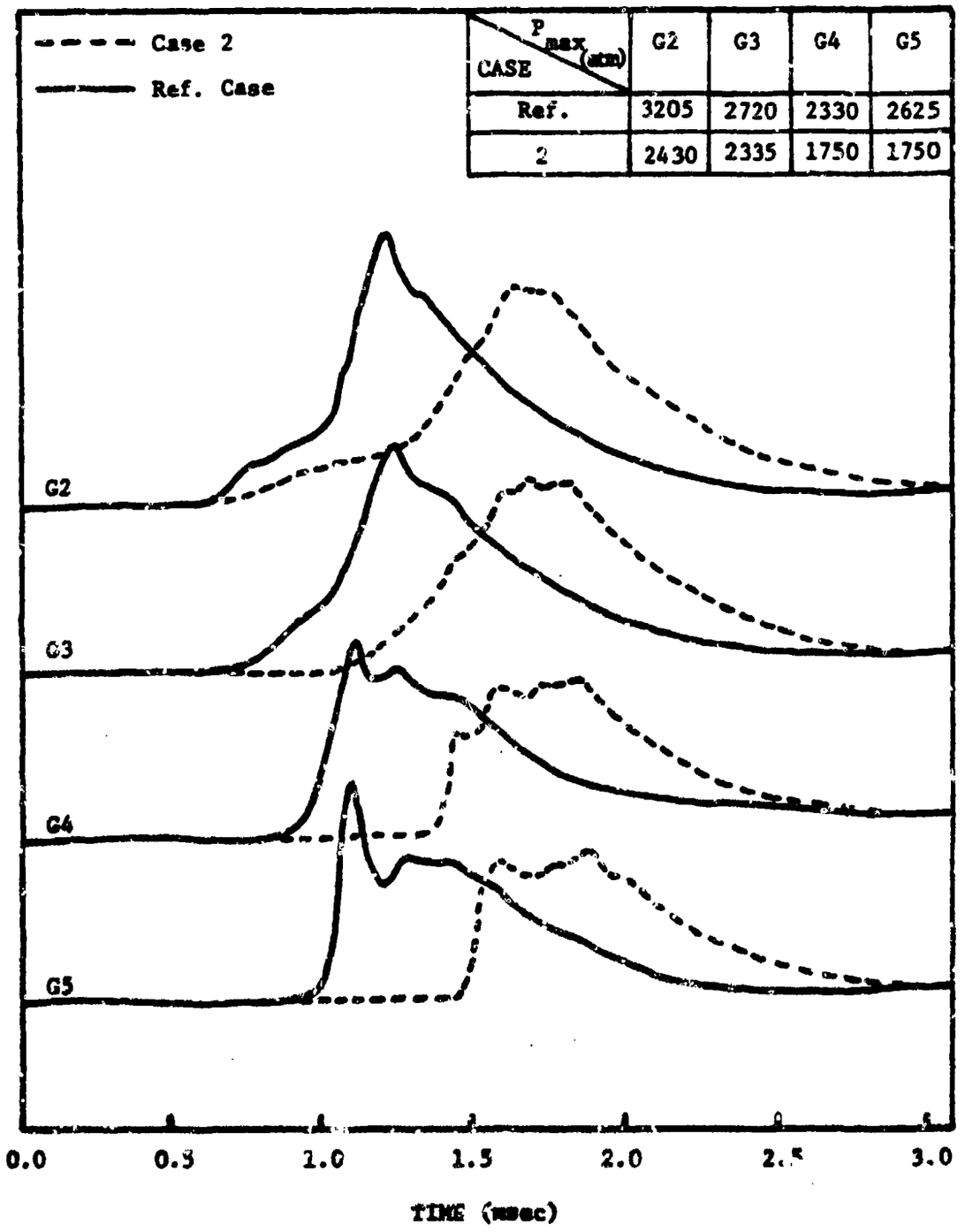

CASE \ P_{max} (atm)	G2	G3	G4	G5
Ref.	3205	2720	2330	2625
2	2430	2335	1750	1750

Figure 17 Comparison of Pressure-Time Traces for Case 2 and the Reference Case

4.2.2 Effect of Propellant Type and Deterrent Concentration

One of the most important elements that can influence mass consumption rates and pressure-time histories for interior ballistics is the particle geometry and the burning rate of the propellant itself. It is not within the scope of this study to develop a relation between propellant physicochemical properties and burning characteristics. The purpose of this section is, however, to compare the data obtained for two additional propellants with the reference case, and briefly point out any significant characteristics for each propellant type.

4.2.2.1 Case 3: WC-846 Deterred Propellant

Shown in Fig. 18 is a typical set of data using WC-846 deterred propellant with an FA-34 primer and 0.81 mm shear disc in the 15.24 cm, 30 caliber combustion chamber. The properties of the Case 3 propellant are listed in Table 4. The results of test firings for Case 3 show a significant acceleration of the pressure front as it travels through the propellant bed. In addition, the peak pressures for Case 3 are consistently higher than those of the reference case. A comparison of the pressure-time data for Case 3 and the reference case is given in Fig. 19. In evaluating these phenomena, it is important to consider the particle geometries. The WC 870 (reference case) propellant is a spherical grain with a maximum diameter of 0.0965 cm and a loading weight in the 15.24 cm combustor of about 7.0 gm. The WC 846 propellant has a cylindrical-disc shape with a maximum particle diameter of 0.0686 cm and a loading weight approximately 9.4% greater than the reference case. This difference in particle geometry has two

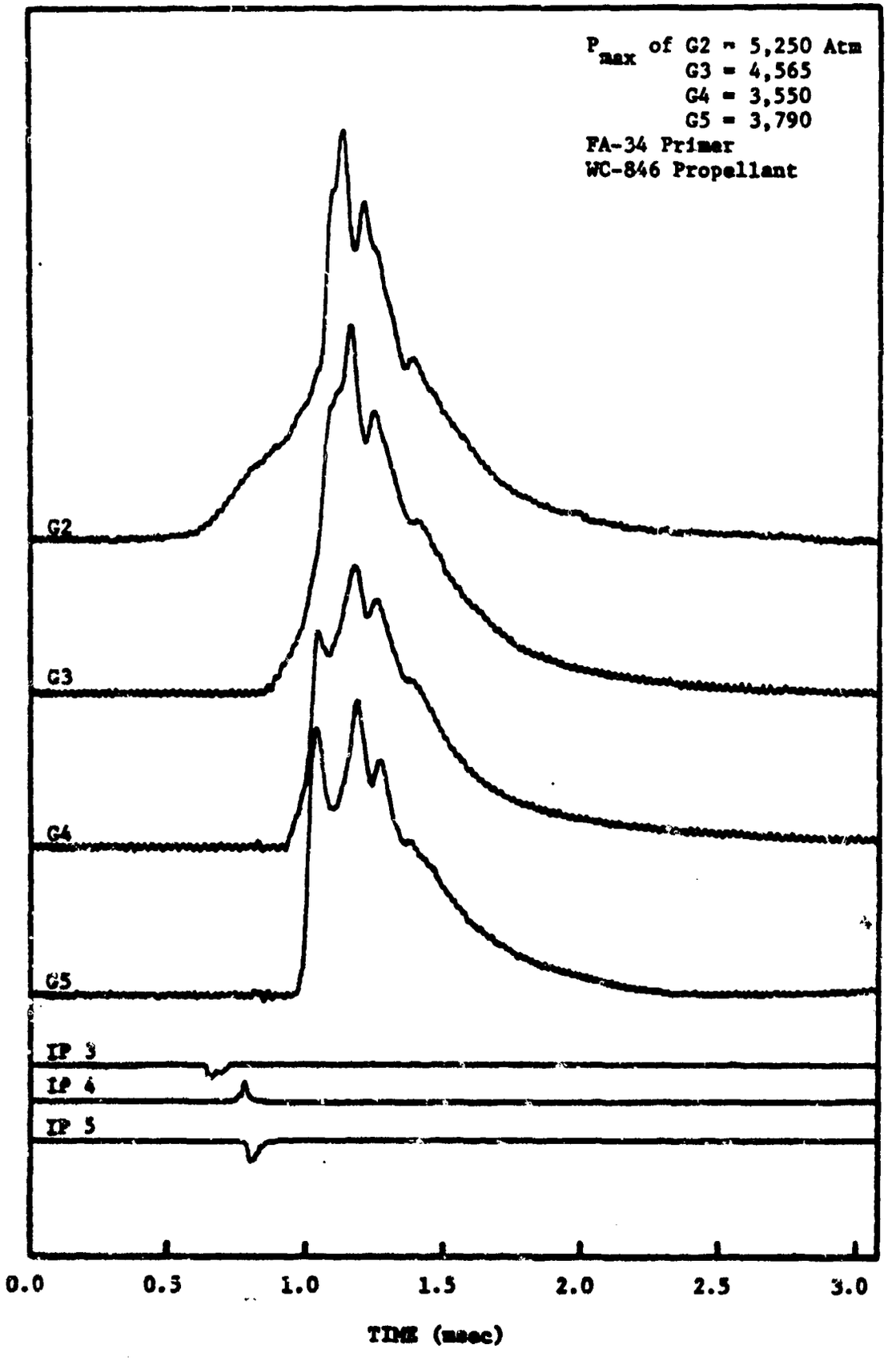

Figure 18 Typical Pressure-Time and Flame Spreading Data for a Case 3 Test Firing (DAP Test No. 89)

TABLE 4

PHYSICAL, COMPOSITIONAL AND THERMO-CHEMICAL DATA
OF WC 846 PROPELLANT*

Particle Shape = Cylindrical-disc

Granulation
Max Particle Diameter = 0.0686 cm
Min Particle Diameter = 0.0406 cm
Web (thickness) = 0.0381 cm

Gravimetric Density = 0.980 gm/cc

% Nitroglycerin = 10.0

% Nominal Nitrogen
Content of Nitrocellulose = 13.15

% Deterrent Coating = 4.9

Heat of Explosion = 883 cal/gm

Flame Temperature = 2,858 °K

*This WC 846 Propellant was manufactured by Olin Corporation, Winchester Group

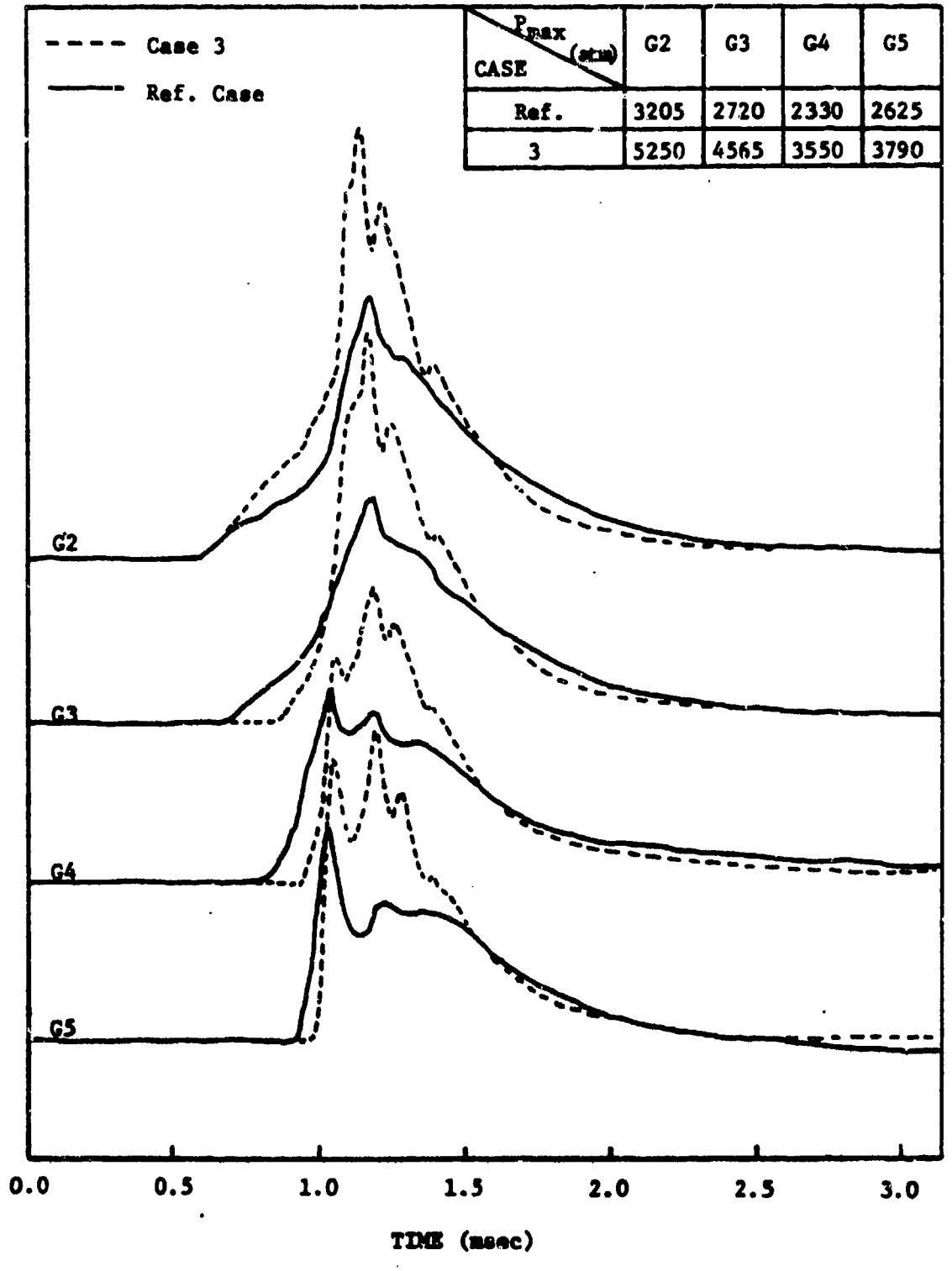

P_{max} (atm) / CASE	G2	G3	G4	G5
Ref.	3205	2720	2330	2625
3	5250	4565	3550	3790

Figure 19 Comparison of Pressure-Time Traces for Case 3 and the Reference Case

significant effects on the initial state of the propellant bed: (1) the smaller WC 846 propellant results in a smaller initial porosity of the granular bed, and (2) the cylindrical-disc shape of the WC 846 grain offers a larger wetted propellant area per unit volume of the propellant particles.

The larger wetted surface area will necessarily increase the total gasification rate of the propellant and thereby increase the pressurization rate within the bed. In addition, the smaller porosity means a smaller void volume within the propellant bed and results in correspondingly higher peak pressures.

4.2.2.2 Case 4: WC-846 Undeterred Propellant

In the theoretical modeling of combustion processes, one of the most difficult problems is to accurately specify the propellant deterrent concentration which is a critical input to the computer solution of the model. This is because the detailed distribution and thickness of deterrent coating on the particle grains is currently unknown. As a result, propellant burning rate as a function of instantaneous particle radius is also unknown. The objective here is to show the drastic changes in pressure-time data when the deterrent coating is not present on the surface of the propellant grain, and the need for concentrated studies in this area.

Figure 20 shows a comparison of the pressure-time histories for the 5% deterred (Case 3) and the undeterred (Case 4) WC-846 propellant. This direct comparison shows that the burning characteristics for the undeterred propellant are much more energetic than the deterred

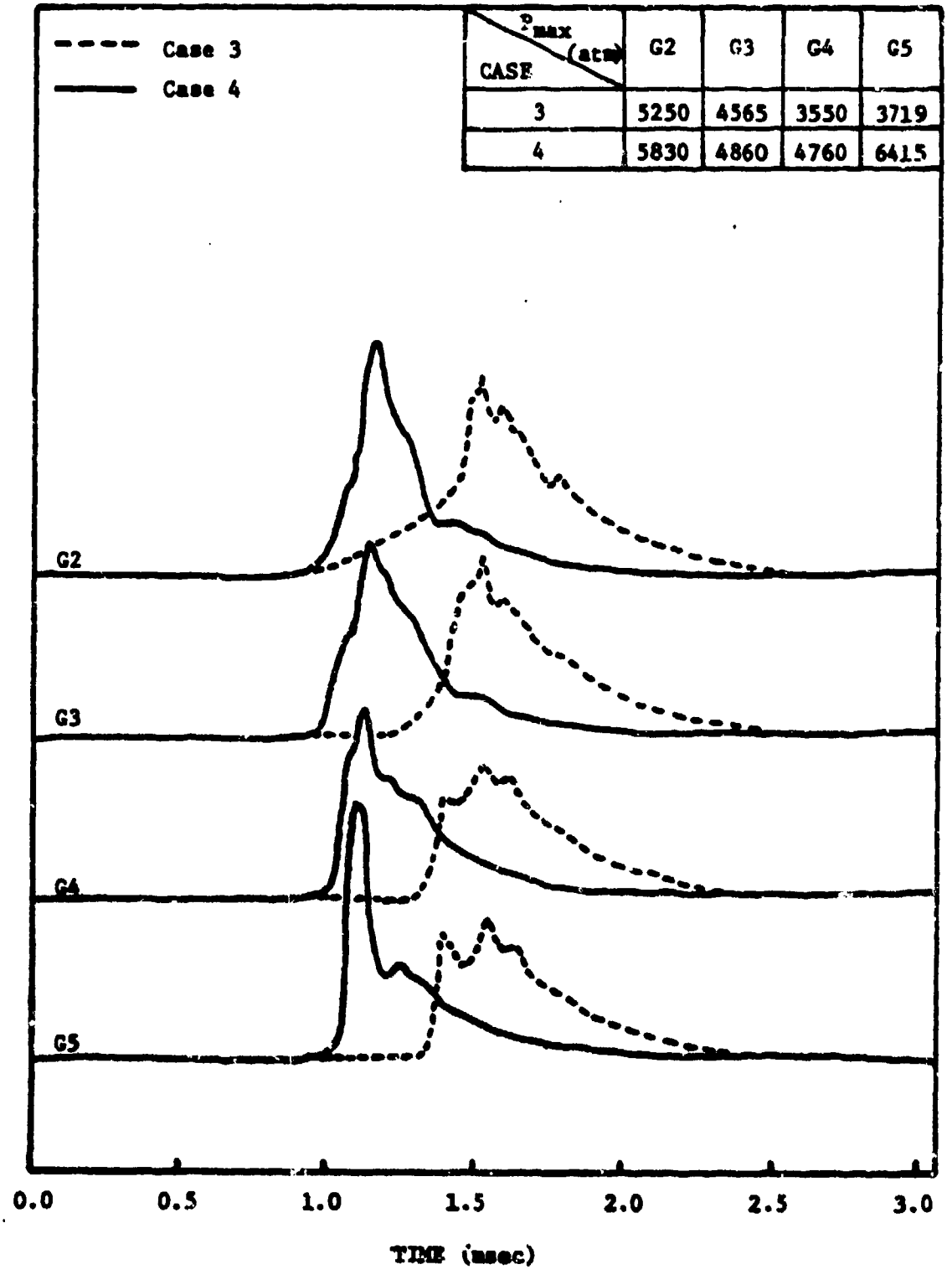

P_{max} (atm) / CASE	G2	G3	G4	G5
3	5250	4565	3550	3719
4	5830	4860	4760	6415

Figure 20 Comparison of Pressure-Time Traces for Cases 3 and 4

propellant. This can be seen by comparing the pressure slopes at the upstream gauge locations (G2, G3). Indeed, the pressure wave travels through the undeterred propellant bed in approximately 70 μsec which can almost be considered as an isochronic ignition of the entire bed. The pressure wave for the deterred propellant takes about six times longer to travel from G2 to G5. The pressure levels for Case 4 are significantly higher than for Case 3 especially at the G5 position. This extreme pressure peak is probably caused by the finite time required for the shear disc to rupture; since the pressure wave is so steep and moving so fast, the rupture of the shear disc occurs at a much higher pressure than for the slower cases. As a result of this extreme pressure level, the rarefaction wave generated by the shear disc motion is much more pronounced, and causes a rapid depressurization at the G5 and G4 locations.

Clearly, the percentage of deterrent content in the propellant grains can drastically affect the entire combustion event. To accurately model flame spreading and combustion processes in a granular bed of deterred propellants, more accurate information about deterrent concentration distribution and propellant burning rate as a function of pressure and deterrent concentration is required.

4.2.3 Effect of Downstream Boundary

In order to more realistically simulate a gun system, the venting shear disc at the downstream boundary was replaced by a projectile and a 27.5 cm gun barrel as shown in Fig. 1. The shear disc remained

in the new configuration (attached to the projectile) in order to permit a pressure build-up within the chamber before motion of the projectile. This set-up provides a transient increase in volume of the combustion chamber during the combustion event.

4.2.3.1 Case 5: Moving Projectile

A typical data set for a test firing using a sliding projectile is given in Fig. 21. In addition to pressure and flame spreading data, the Case 5 tests also include projectile displacement measurements. The physical arrangement for the phototransistors has been given in Section 3.5. It should be noted that the time of arrival of the projectile at each measurement position is given by the first discernible rise in voltage for each phototransistor pulse.

In Fig. 21, the flame spreading data indicate a slight acceleration of the flame front and also of the pressure front as they travel through the bed. The projectile displacement data indicate a rapid acceleration of the projectile followed by a slight deceleration as it nears the muzzle of the projectile chamber. This deceleration is accompanied by a decrease in pressure in the combustion chamber (G2-G5).

A comparison of Case 5 and the reference case is shown in Fig. 22. This direct comparison shows that the initial portion of both curves at each gauge location agree quite closely. The effect of the piston is most obvious after the time the shear disc has ruptured. Both cases indicate the effect of the rarefaction wave which is generated by the rupture and subsequent motion of the downstream boundary (G4, G5). However, the Case 5 data for G4 and G5 show a pronounced second peak

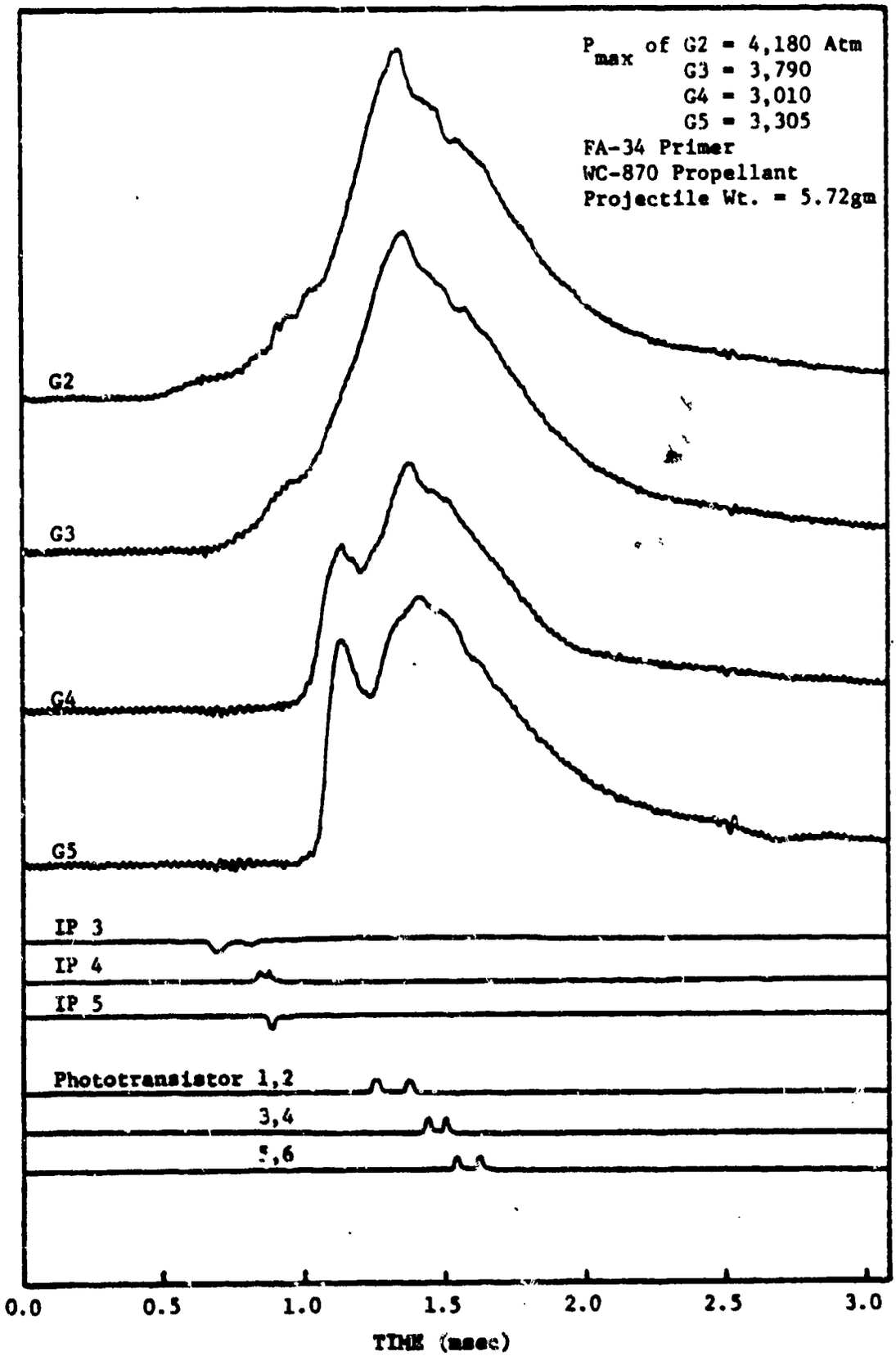

Figure 21 Typical Pressure-Time, Flame Spreading, and Projectile Data for a Case 5 Test Firing (DAP Test No. 86)

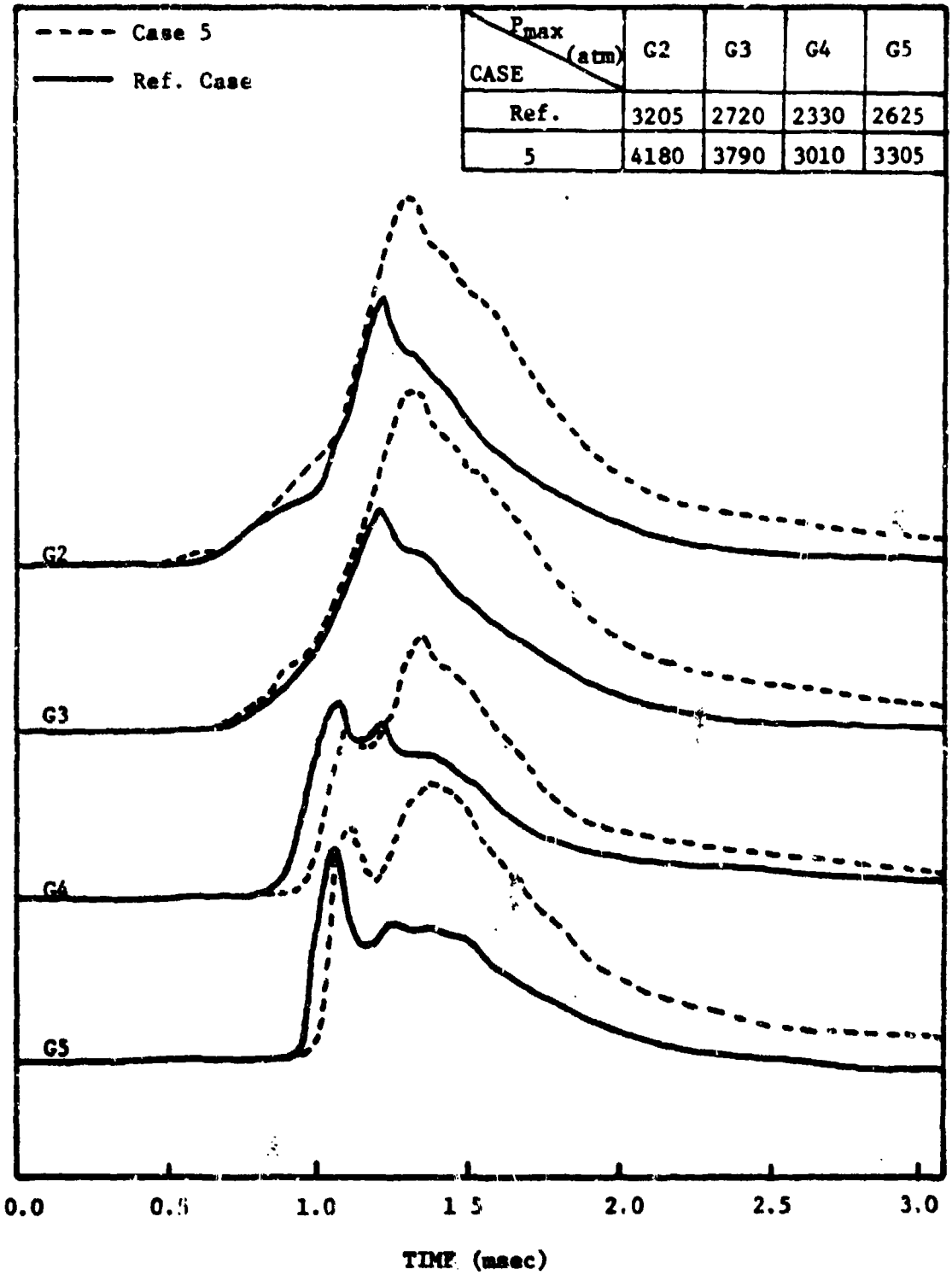

Figure 22 Comparison of Pressure-Time Traces for Case 5 and the Reference Case

which is significantly higher than the first. This higher peak is caused by the continued gasification of propellant behind the projectile. In addition, the momentary dip in pressure at G4 and G5 is not as great as that for the reference case because of the inertia of the projectile; the projectile of Case 5 accelerates less rapidly than the light shear disc of the reference case, thereby generating a less pronounced rarefaction wave which travels back through the bed.

Since the projectile travels through the projectile chamber in approximately 0.5 msec, the Case 5 combustion process remains partially confined for that time period, resulting in a much slower pressure decay than that for the reference case.

4.2.4 Comparison of the Locus of Pressure Fronts

The pressure wave development for the various cases observed in this study can be summarized by considering the plots of pressure front loci shown in Figs. 23 and 24. Although the induction time for each case is different, for the purpose of this comparison the first discernible pressure rise at G2 for each case is designated as time equal to zero.

Figure 23 shows the effect of igniter strength on the velocity of pressure front propagation through the bed. Case 1 propagates with the lowest velocity due to the combination of a weak igniter and large gaseous igniter volume. Case 2 also has a weak igniter (FA-41) but due to the small primer volume, the pressure front accelerates rapidly in the downstream portion of the granular bed. The reference case combines a strong igniter (FA-34) with a small primer volume to produce a relatively high velocity pressure front.

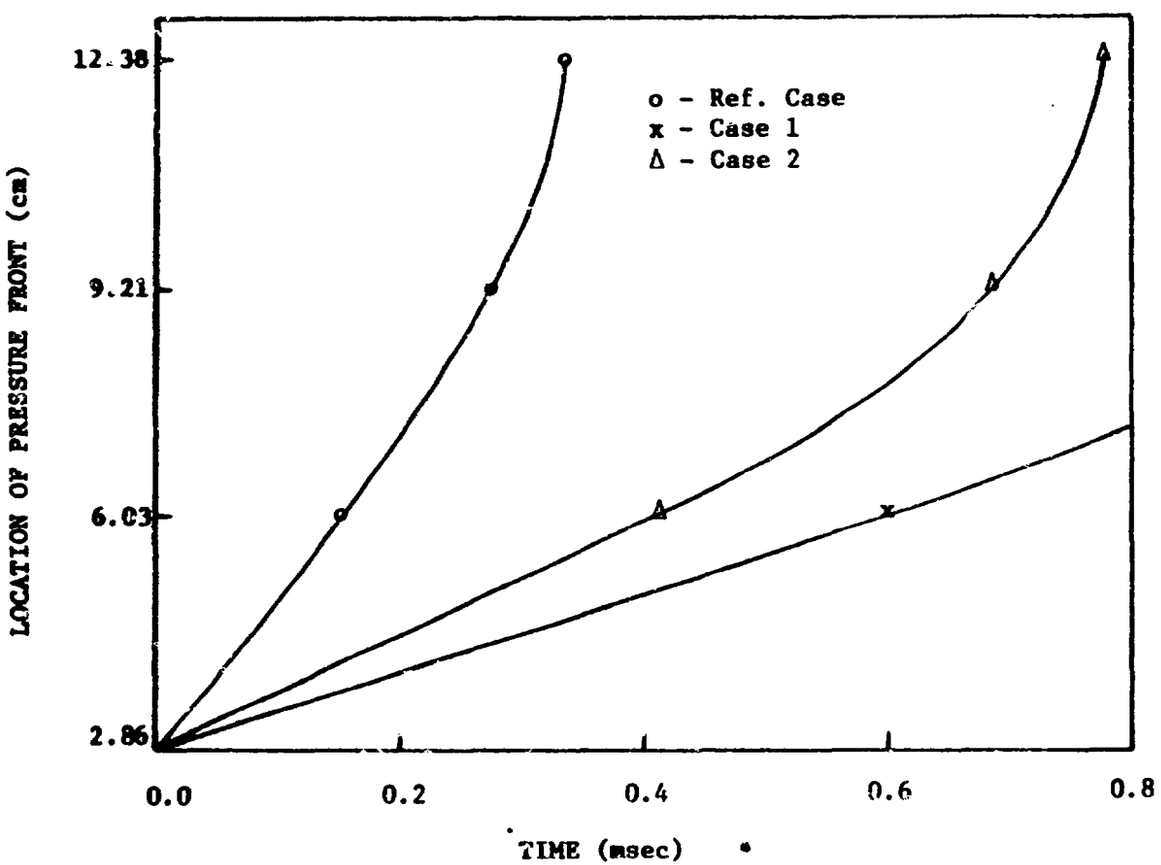

Figure 23 Comparison of Pressure Front Loci for Cases 1, 2, and the Reference Case

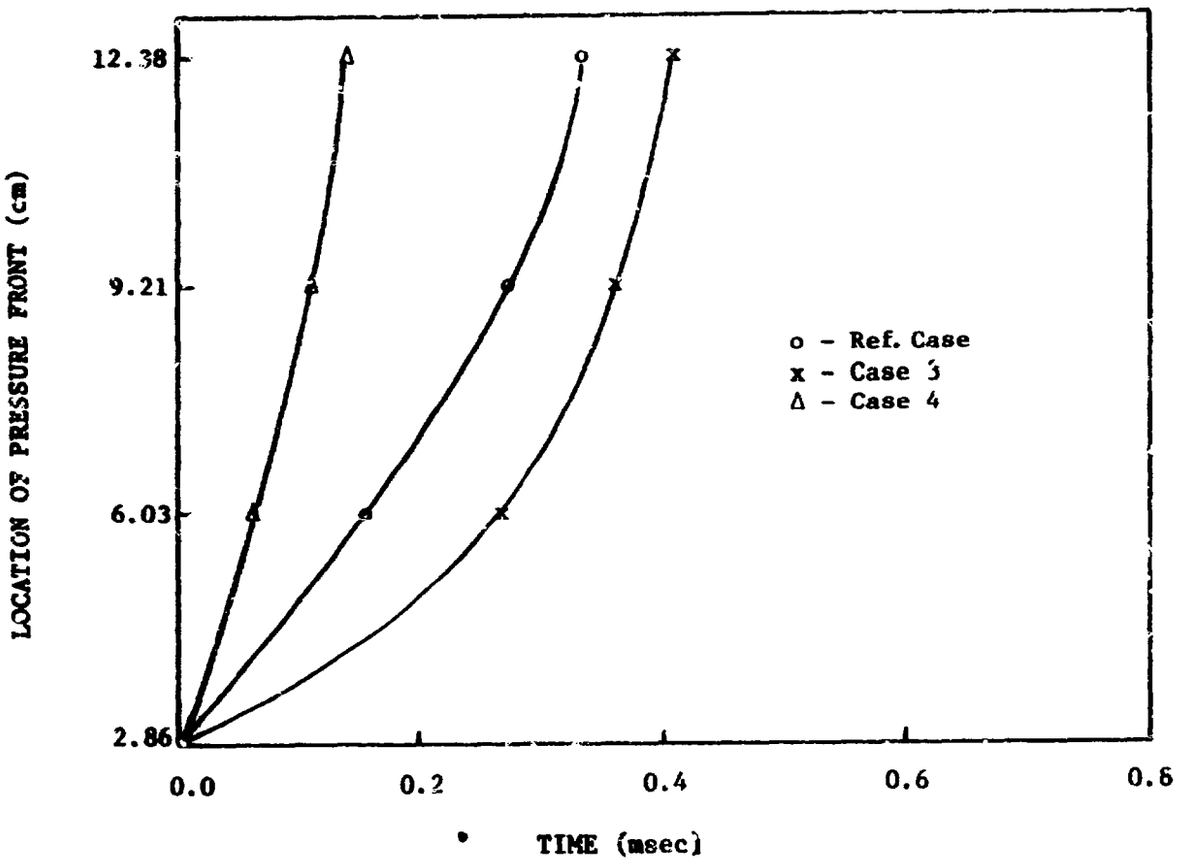

Figure 24 Comparison of Pressure Front Loci for Cases 3, 4, and the Reference Case

Figure 24 shows the effect of propellant type on the propagation velocity of pressure front through the bed. For Case 3 (WC 846), the velocity of the pressure front initially propagates with the lowest velocity primarily due to a lower initial porosity of the granular bed. However, it accelerates rapidly and eventually approaches the velocity of the reference case. For Case 4 (undeterred WC 846), the velocity of the pressure front propagates with the highest velocity and approaches a near isochronic ignition of the entire granular bed.

CHAPTER V

CONCLUSIONS

An experimental investigation has been conducted to study the effects of primer strength, propellant type, and downstream boundary on the transient combustion processes in granular propellant beds. During the course of this study, an experimental test rig has been designed and fabricated. Also, a data acquisition system has been developed to measure the transient pressurization, flame spreading, and projectile motion with a time resolution of five micro seconds.

Several important conclusions of this investigation are summarized below:

1. The igniter strength significantly affects the transient combustion processes in granular propellant beds. A weak primer which causes less bed compaction was found to produce the following effects:

   a) a longer induction period before ignition of the bed; and

   b) a pronounced pressure front acceleration.

   In addition, a large igniter volume was found to cause significant back flow of product gases, thereby retarding the flame spreading and pressurization processes.

2. Propellant deterrent concentration drastically affects the overall combustion and flame spreading processes. Undeterred propellant was found to cause:

   a) extremely rapid flame spreading due to rapid ignition of propellant particles

   b) higher peak pressures due to higher gasification rates

   c) extremely high downstream pressurization rates due to the extremely high velocity of the pressure front.

3. A larger propellant wetted surface area per unit volume produces an increased rate of total mass consumption, resulting in more pronounced pressure wave phenomena within the granular propellant bed.

4. A moving downstream boundary produces the following effects which are different from the vented chamber configuration:

   a) continued gasification of propellant behind the moving projectile, resulting in a maximum peak pressure after the projectile has started in motion; and

   b) a longer time interval for the depressurization of the chamber.

5. An experimental test facility, including test rig and data acquisition system, has been developed to study a wide variety of combustion conditions. The test facility has the capability to detect and record the rapid transients that are characteristic of granular propellant combustion.

ACKNOWLEDGMENTS

This report represents the experimental results of the research work performed under contract DAAG 29-74-G-0116 at The Pennsylvania State University, under the supervision of the Engineering Sciences Division of the U.S. Army Research Office at Research Triangle Park, North Carolina. The support of Mr. James J. Murray, Director of Engineering Sciences Division, and of Dr. Austin W. Barrows, Jr. of the Ballistic Research Laboratories is greatly appreciated. Thanks are due to Mr. Norman J. Gerri of BRL for his technical advice throughout this study; to Mr. Richard H. Comer of BRL who authorized the supply of granular propellant used in our work; and to Dr. Richard R. Bernecker of NSWC/WOL for providing us with technical information about ionization pins.

We would also like to thank our machinist, Mr. James A. Lauck, and undergraduate assistants, Mr. Irvin P. Troutman and Mr. William C. Morris. for their laboratory assistance; and a special thanks to Miss Susan L. Walker who typed this manuscript.

REFERENCES

1. Kuo, K.K., "Theory of Flame Front Propagation in Porous Propellant Charges Under Confinement," Ph.D. Thesis, Princeton Univ., AMS RN 1000-T, pp. 73-80, 1971.

2. Kuo, K.K., Vichnevetsky, R. and Summerfield, M., "Theory of Flame Front Propagation in Porous Propellant Charges under Confinement," AIAA Journal, Vol. 11, No. 4, pp. 444-451, 1973.

3. Kuo, K.K. and Summerfield, M., "Theory of Steady-State Burning of Gas-Permeable Propellants," AIAA Journal, Vol. 12, No. 1, pp. 49-56, 1974.

4. Kuo, K.K. and Summerfield, M., "High Speed Combustion of Mobile Granular Solid Propellants: Wave Structure and the Equivalent Rankine-Hugoniot Relation," Fifteenth (International) Symposium on Combustion, pp. 515-527, 1974.

5. Koo, J.H., "Theoretical Modeling and Numerical Solution of Transient Combustion Processes in Mobile Granular Propellant Beds," M.S. Thesis, Mechanical Engineering Department, The Pennsylvania State University, University Park, Pennsylvania, 1975.

6. Kuo, K.K., Koo, J.H., Davis, T.R. and Coates, G.R., "Transient Combustion in Mobile Gas-Permeable Propellants," Acta Astronautica, Vol. 3, pp. 573-591, 1976.

7. Kuo, K.K. and Coates, G.R., "Review of Dynamic Burning of Solid Propellants in Gun and Rocket Propulsion Systems," presented at the Sixteenth Symposium (International) on Combustion held at the Massachusetts Institute of Technology, Cambridge, Massachusetts, August 15-20, 1976.

8. Kuo, K.K., "A Summary of the JANNAF Workshop on: Theoretical Modeling and Experimental Measurements of the Combustion and Fluid Flow Processes in Gun Propellant Charges," presented at the 13th JANNAF Combustion Meeting held at Naval Postgraduate School, Monterey, California, September 13-17, 1976.

9. Alkidas, A., Morris, S.O., Cavany, L.H. and Summerfield, M., "An Experimental Study of Pressure Wave Propagation in Granular Propellant Beds," AIAA J., Vol. 14, No. 6, pp. 789-792, 1976.

10. Gerri, N.J., Samuel, P.P. and Ortega, A.E., "Gas Flow in Porous Beds of Packed Ball Propellant," BRL IMR 159, Ballistic Research Laboratories, Aberdeen Proving Ground, Maryland, 1973.

11. Gough, P.S., "The Flow of a Compressible Gas Through an Aggregate of Mobile Reacting Particles," Ph.D. Thesis, Mech. Engr. Dept., McGill University, Montreal, Quebec, Canada, 1974.

12. Gough, P.S., "Fundamental Investigation of the Interior Ballistics of Guns," Final Report IHCR 74-1, Naval Ordnance Station, Indian Head, Maryland, 1974.

13. Kitchens, C.W., Jr. and Gerri, N.J., "Numerical and Experimental Investigation of Flame Spreading and Gas Flow in Gun Propellants," presented in JANNAF Safety Meeting on Combustion, 1973.

14. Krier, H., Van Tassell, W., Rajan, S., VerShaw, J.T., "Model of Gun Propellant Flame Spreading and Combustion," BRL CR 147, Ballistic Research Laboratories, Aberdeen Proving Ground, Maryland, 1974. (AD #918842L)

15. Krier, H., Rajan, S., Van Tassell, W.F., "Flame-Spreading and Combustion in Packed Beds of Propellant Grains," AIAA J., Vol. 14, No. 3, pp. 301-309, 1976.

16. Fisher, E.B., Graves, K.W., "Mathematical Model at Double Base Propellant Ignition and Combustion in the 81 mm Mortar," CAL Report No. DG-3029-D-1, August 1972.

17. Fisher, E.B., Trippe, A.P., "Development of a Basis for Acceptance of Continuously Produced Propellant," Calspan Report No. VQ-5163-D-1, November 1973.

18. Fisher, E.B. and Trippe, A.P., "Mathematical Model of Center Core Ignition in the 175 mm Gun," Calspan Report No. VQ-5163-D-2, March 1974.

19. Fisher, E.B., "Propellant Ignition and Combustion in the 105 mm Howitzer," Calspan Report No. VQ-5524-D-1, 1975.

20. Kooker, D.E., Nelson, C.W., "Numerical Solution of Three Solid Propellant Combustion Models during a Gun Pressure Transient," 12th JANNAF Combustion Meeting, Newport, Rhode Island, 1975.

21. Nelson, C.W., "Response of Three Types of Transient Combustion Models to Gun Pressurization," BRL IMR No. 447, October 1975.

22. Soper, W.G., "Grain Velocities During Ignition of Gun Propellant," Combustion and Flame, Vol. 24, No. 2, pp. 199-202, 1975.

23. Squire, W.H. and Divene, M.P., "The Interface Between Primer and Propellant," Part I and II, United States Army, Frankford Arsenal, Philadelphia, Pennsylvania, 1969.

24. Warlick, G.L., "Ignition-Produced, Shock-Loading Phenomena in Naval Guns," CPIA Publication 220, 8th JANNAF Combustion Meeting, Vol. 1, September 1971.

25. Gerri, N.J., Pfaff, S.P. and Ortega, A.E., "Gas Flow in Porous Beds of Packed Propellant," BRL IMR 159, Ballistic Research Laboratories, Aberdeen Proving Ground, Maryland, 1973.

26. Gerri, N.J. and Pfaff, S.P., "Gas Flow and Flame Spreading in a 20.16 cm Bed of Porous Propellant," BRL IMR 420, Ballistic Research Laboratories, Aberdeen Proving Ground, Maryland, 1975.

27. Bernecker, R.R. and Price, D., "Studies in the Transition from Deflagration to Detonation in Granular Explosives - I. Experimental Arrangement and Behavior of Explosives which Fail to Exhibit Detonation," Combustion and Flame, Vol. 22, No. 1, pp. 111-118, February 1974.

28. Bernecker, R.R. and Price, D., "Studies in the Transition from Deflagration to Detonation in Granular Explosives - II. Transitional Characteristics and Mechanisms Observed in 91/9 RDX/WAX," Combustion and Flame, Vol. 22, No. 1, pp. 119-129, February 1974.

29. Bernecker, R.R. and Price D., "Studies in the Transition from Deflagration to Detonation in Granular Explosives - III. Proposed Mechanisms for Transition and Comparison with Other Proposals in the Literature," Combustion and Flame, Vol. 22, No. 2, pp. 161-170, April 1974.

30. Horst, A.W., "Solid Propellant Gun Interior Ballistics Annual Report: FY-75," IHTR 441, Naval Ordnance Station, Indian Head, Maryland, 1976.

31. Horst, A.W., "Influence of Propellant Burning Rate Representation on Gun Environment Flame Spread and Pressure Wave Predictions," IHMR 76-255, Naval Ordnance Station, Indian Head, Maryland, 1976.

32. Horst, A.W., Smith, T.C. and Mitchell, S.E., "Experimental Evaluation of Three Concepts for Reducing Pressure Wave Phenomena in Navy 5-inch, 54 Caliber Guns: Summary of Firing Data," IHMR 76-258, Naval Ordnance Station, Indian Head, Maryland, 1976.

33. East, J.L. and McClure, D.R., "Experimental Studies of Ignition and Combustion in Naval Guns," Proceedings 12th JANNAF Combustion Meeting, August 1975.

34. Cavony, L.H. and Summerfield, M., "Combustion Characteristics of Individual Grains of Multi-perforated Propellant," Presentation to JANNAF Workshop on Gun Propellant Combustion, Newport, Rhode Island, August 1975.

35. Alkidas, A.C., Morris, S.O., Carreny, L.H. and Summerfield, M., "Experimental Study of Pressure Wave Propagation in Granular Propellant Beds," AIAA Journal, Vol. 14, No. 6, pp. 789-792, June 1976.

36. Brosseau, T.L., "Development of the Minihat Pressure Transducer for Use in the Extreme Environments of Small Caliber Gun Barrels," BRL MR 2072, Ballistic Research Laboratories, Aberdeen Proving Ground, Maryland, November 1970. (AD #878325)

37. Norton, H.N., Handbook of Transducers for Electronic Measuring Devices, Prentice-Hall, Inc., Englewood Cliffs, New Jersey, pp. 414-508, 1969.

38. Gibson, R.W. and Macek, A., "Flame Fronts and Compression Waves during Transition from Deflagration to Detonation in Solids," Eighth Symposium (International) on Combustion, pp. 847-854, 1959.

39. Stansbury, L. and Comer, R.H., "Electronic and Numerical Techniques for Reducing Noisy Gun Ballistic Data," BRL MR 2492, Ballistic Research Laboratories, Aberdeen Proving Ground, Maryland, June 1975. (AD #B0061451.)

40. Schlack, A., Private communication with K.K. Kuo between Frankford Arsenal and the Pennsylvania State University, October 1976.

APPENDIX I

GENERAL REFERENCE OF PRESSURE TRANSDUCER TYPES AND SENSING ELEMENTS

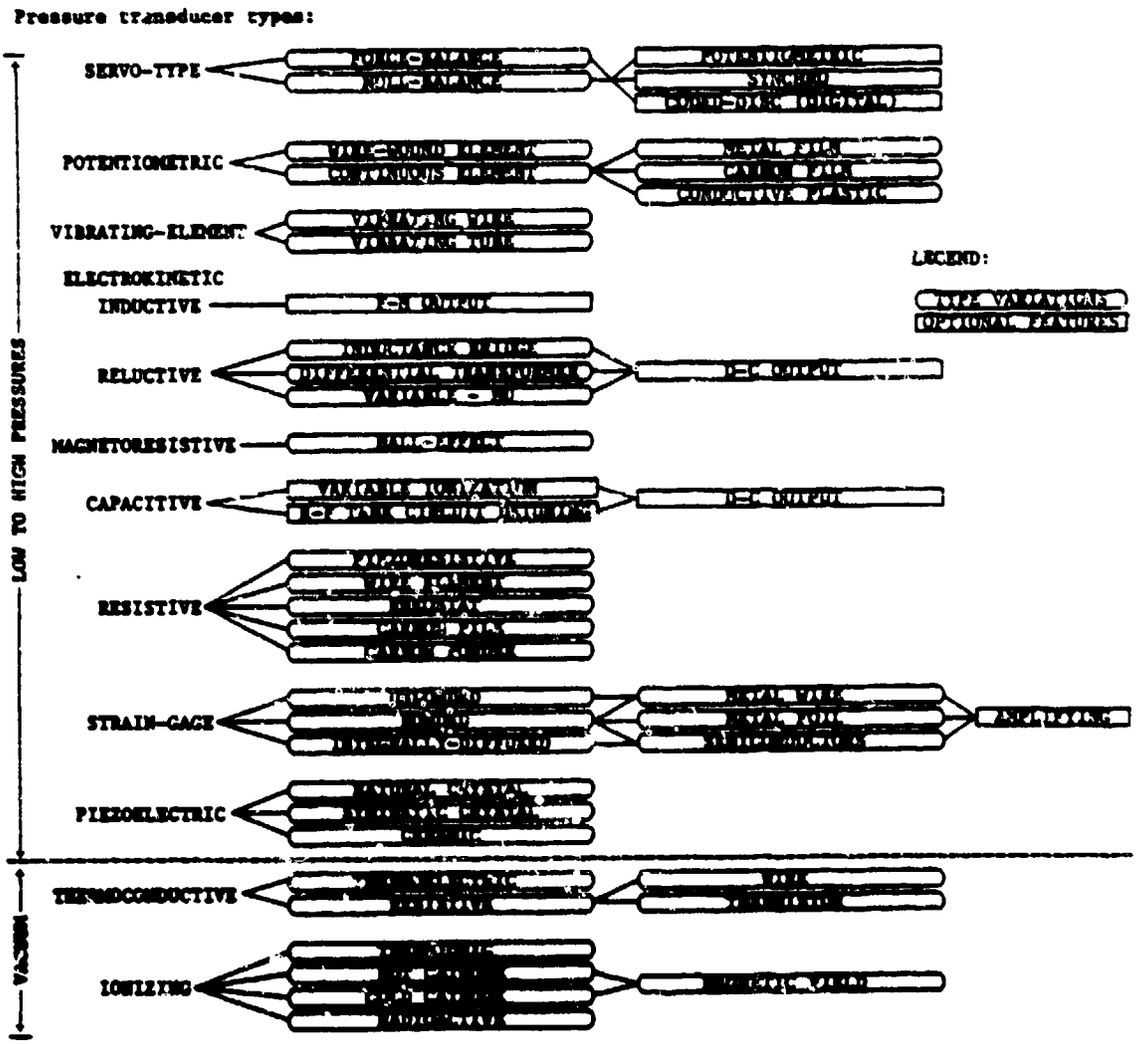

Pressure sensing elements:

a) FLAT DIAPHRAM

b) CORRUGATED DIAPHRAM

c) CAPSULE

d) BELLOWS

e) STRAIGHT TUBE

f) C-SHAPED BOURDON TUBE

g) TWISTED BOURDON TUBE

h) HELICAL BOURDON TUBE

i) SPIRAL BOURDON TUBE

APPENDIX II: WIRING DIAGRAM OF THE DATA ACQUISITION SYSTEM

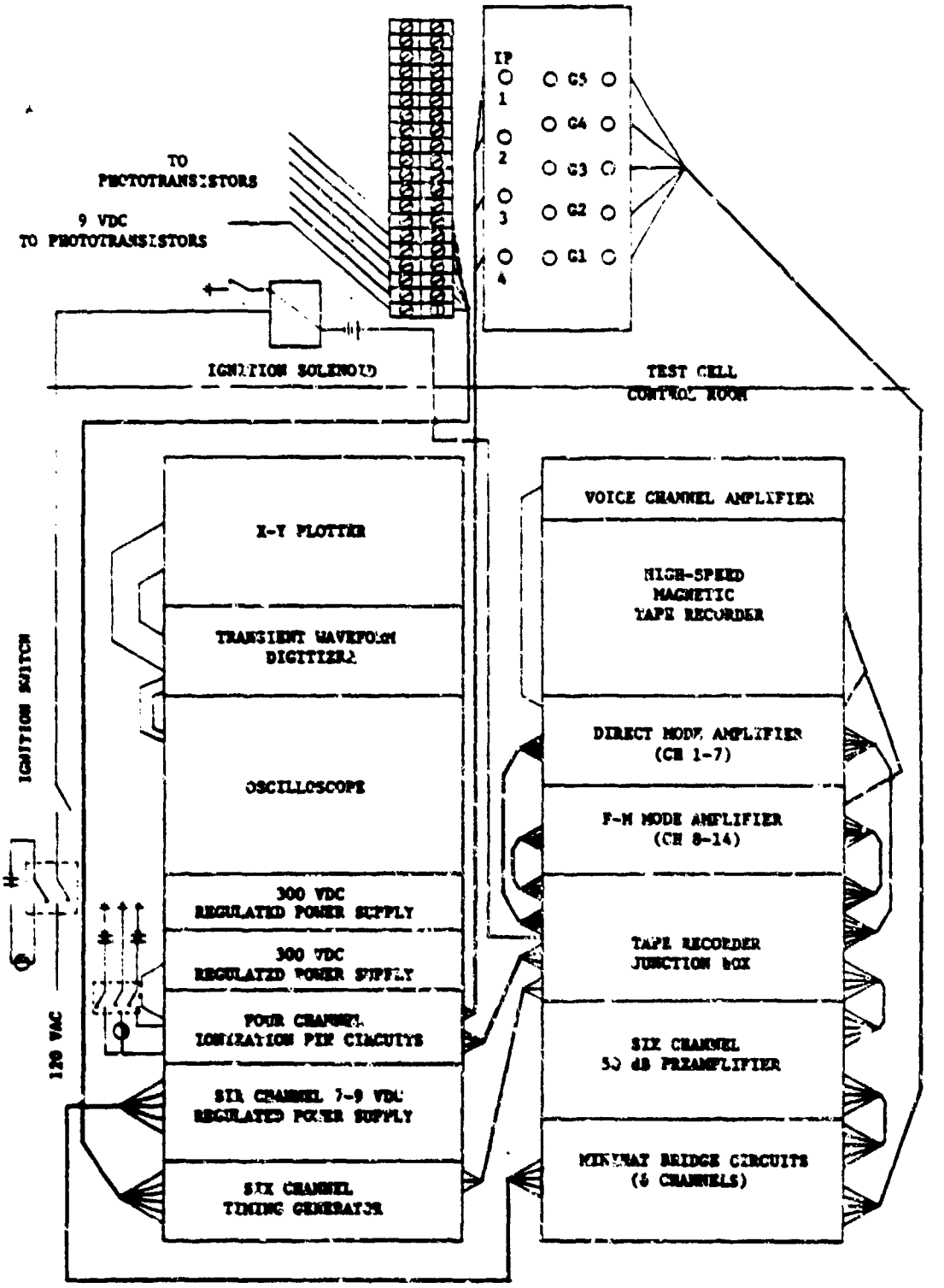

DISTRIBUTION LIST

No. of Copies	Organization
12	Commander Defense Documentation Center ATTN: DCC-TCA Cameron Station Alexandria, VA 22314
1	Director Defense Advanced Research Projects Agency ATTN: C. R. Lehner 1400 Wilson Boulevard Arlington, VA 22209
2	Director Institute for Defense Analyses ATTN: Dr. H. Wolfhard Mr. R. T. Oliver 400 Army-Navy Drive Arlington, VA 22202
1	Commander US Army Materiel Development and Readiness Command ATTN: DRCDMA-ST 5001 Eisenhower Avenue Alexandria, VA 22333
1	Commander US Army Aviation Systems Command ATTN: DRSAV-E 12th and Spruce Streets St. Louis, MO 63166
1	Director US Army Air Mobility Research and Development Laboratory Ames Research Center Moffett Field, CA 94035
1	Commander US Army Electronics Command ATTN: DRSEL-RD Ft. Monmouth, NJ 07703
1	Commander US Army Missile Research and Development Command ATTN: DRDMI-R Redstone Arsenal, AL 35809
1	Commander US Army Tank Automotive Development Command ATTN: DRDTA-TWL Warren, MI 48090
2	Commander US Army Mobility Equipment Research & Development Command ATTN: Tech Doc Ctr, Bldg 315 DRSME-RZT Ft. Belvoir, VA 22060
1	Commander US Army Armament Materiel Readiness Command Rock Island, IL 61202
8	Commander US Army Armament Research and Development Command ATTN: DRDAR-LC, Dr. H. Fair DRDAR-LCE, Mr. C. Lenchitz DRDAR-LCE, Dr. R. F. Walker DRDAR-LCE, Dr. J. Hershkowitz F. Fitzsimmons P. A. Serao J. Domen J. C. Pearson Dover, NJ 07801
1	Commander US Army White Sands Missile Range ATTN: STEWS-VT WSMR, NM 88002

DISTRIBUTION LIST

No. of Copies	Organization
1	Commander US Army Watervliet Arsenal ATTN: R. Thierry/Code SARWV-RD Watervliet, NY 12189
1	Commander US Army Harry Diamond Labs ATTN: DRXDO-TI 2800 Powder Mill Road Adelphi, MD 20783
1	Commander US Army Materials and Mechanics Research Center ATTN: DRXMR-ATL Watertown, MA 02172
1	Commander US Army Natick Research and Development Command ATTN: DRXRE, Dr. D. Sieling Natick, MA 01762
1	Director US Army TRADOC Systems Analysis Activity ATTN: ATAA-SA WSMR, NM 88002
1	Commander US Army Research Office ATTN: Tech Lib P.O. Box 12211 Research Triangle Park, NC 27706
1	Chief of Naval Research ATTN: Code 473 800 N. Quincy Street Arlington, VA 22217
1	Commander US Naval Sea Systems Command ATTN: J. W. Murrin (NAVSEA-0331) National Center, Bldg 2, Rm 6E08 Washington, DC 20360
2	Commander US Naval Surface Weapons Ctr ATTN: S. J. Jacobs/Code 240 Code 730 Silver Spring, MD 20910
1	Commander US Naval Surface Weapons Ctr ATTN: Tech Lib Dahlgren, VA 22338
1	Commander US Naval Underwater Systems Ctr Energy Conversion Department ATTN: R. S. Lazar/Code 5B331 Newport, RI 02840
2	Commander US Naval Weapons Center ATTN. Dr. R. Derr Mr. C. Thelen China Lake, CA 93555
1	Commander US Naval Research Laboratory ATTN: Code 6180 Washington, DC 20375
3	Superintendent US Naval Postgraduate School ATTN: Tech Lib Dr. David Netzer Dr. Allen Fuhs Monterey, CA 93940
2	Commander US Naval Ordnance Station ATTN: Dr. A. Roberts Tech Lib Indian Head, MD 20640
2	AFOSR ATTN: J. R. Masi Dr. B. T. Wolfson Bolling AFB, DC 20332

DISTRIBUTION LIST

No. of Copies	Organization
2	AFRPL (DYSC) ATTN: Dr. D. George Mr. J. N. Levine Edwards AFB, CA 93523
1	Lockheed Palo Alto Rsch Labs ATTN: Tech Info Ctr 3521 Hanover Street Palo Alto, CA 94304
1	National Science Foundation ATTN: Dr. Morris Ojalvo Washington, DC 20550
1	Aerojet Solid Propulsion Co. ATTN: Dr. P. Micheli Sacramento, CA 95813
1	ARO Incorporated ATTN: Mr. S. Dougherty Arnold AFS, TN 37389
1	Atlantic Research Corporation ATTN: Dr. M. K. King 5390 Cherokee Avenue Alexandria, VA 22314
1	AVCO Corporation AVCO Everett Research Lab Div ATTN: D. Stickler 2385 Revere Beach Parkway Everett, MA 02149
2	Calspan Corporation ATTN: Dr. E. B. Fisher A. P. Trippe P.O. Box 235 Buffalo, NY 14221
1	Energy Incorporated ATTN: Dr. E. D. Hughes Idaho Falls, ID 83401
1	ENKI Corporation ATTN: M. I. Madison 9015 Fulbright Avenue Chatsworth, CA 91311
1	Foster Miller Assoc., Inc. ATTN: A. J. Erickson 135 Second Avenue Waltham, MA 02154
1	General Electric Company Armament Department ATTN: M. J. Bulman Lakeside Avenue Burlington, VT 05402
1	General Electric Company Flight Propulsion Division ATTN: Tech Lib Cincinnati, OH 45215
2	Hercules Incorporated Alleghany Ballistic Lab ATTN: Dr. R. Miller Tech Lib Cumberland, MD 21501
2	Hercules Incorporated Bacchus Works ATTN: Dr. M. Beckstead Dr. R. Simmons Magna, UT 84044
2	IITRI ATTN: Dr. M. J. Klein H. Napadensky 10 West 35th Street Chicago, IL 60615
1	Olin Corporation Badger Army Ammunition Plant ATTN: J. Rammarace Baraboo, WI 53913

DISTRIBUTION LIST

No. of Copies	Organization
2	Olin Corporation New Haven Plant ATTN: R. L. Cook D. W. Riefler 275 Winchester Avenue New Haven, CT 06504
1	Paul Gough Associates, Inc. ATTN: Dr. P. S. Gough P.O. Box 1614 Portsmouth, NH 03801
1	Pulsepower Systems, Inc. ATTN: L. C. Elmore 815 American Street San Carlos, CA 94070
1	Science Applications, Inc. ATTN: Dr. R. B. Edelman 23146 Cumorah Crest Woodland Hills, CA 91364
2	Rockwell International Corp. Rocketdyne Division ATTN: Dr. C. Obert Dr. J. E. Flanagan 6633 Canoga Avenue Canoga Park, CA 91304
2	Rockwell International Corp. Rocketdyne Division ATTN: Mr. W. Haynes Tech Lib McGregor, TX 76657
1	Shock Hydrodynamics, Inc. ATTN: Dr. W. H. Anderson 4710-16 Vineland Avenue North Hollywood, CA 91602
1	Thiokol Corporation Elkton Division ATTN: E. Sutton Elkton, MD 21921
3	Thiokol Corporation Huntsville Division ATTN: Dr. D. Flanigan Dr. R. Glick Tech Lib Huntsville, AL 35807
2	Thiokol Corporation Wasatch Division ATTN: Dr. John Peterson Tech Lib P.O. Box 524 Brigham City, UT 84302
1	TRW Systems Group ATTN: Dr. H. Korman One Space Park Redondo Beach, CA 90278
2	United Technology Center ATTN: Dr. R. Brown Tech Lib P.O. Box 358 Sunnyvale, CA 94088
1	Universal Propulsion Co. ATTN: H. J. McSpadden P.O. Box 546 Riverside, CA 92502
1	Battelle Memorial Institute ATTN: Tech Lib 505 King Avenue Columbus, OH 43201
1	Brigham Young University Dept of Chemical Engineering ATTN: Prof. R. Coates Provo, UT 84601

DISTRIBUTION LIST

No. of Copies	Organization
1	California Institute of Tech. Jet Propulsion Laboratory ATTN: Prof. F. E. C. Culick Pasadena, CA 91103
1	California State University ATTN: F. H. Reardon Sacramento, CA 95813
1	Case Western Reserve Univ. Division of Aerospace Sciences ATTN: Prof. J. Tien Cleveland, OH 44135
3	Georgia Institute of Technology School of Aerospace Engineering ATTN: Prof. B. T. Zinn Prof. E. Price Prof. W. C. Strahle Atlanta, GA 30332
1	Institute of Gas Technology ATTN: Dr. D. Gidaspow 3424 S. State Street Chicago, IL 60616
1	Johns Hopkins University Applied Physics Laboratory Chemical Propulsion Information Agency ATTN: Mr. T. Christian Johns Hopkins Road Laurel, MD 20810
1	Massachusetts Institute of Technology Dept of Mechanical Engineering ATTN: Prof. T. Toong Cambridge, MA 02139
1	Pennsylvania State University Applied Research Lab ATTN: Dr. G. M. Faeth P.O. Box 30 State College, PA 16801
1	Pennsylvania State University Dept of Mechanical Engrg ATTN: Prof. K. Kuo University Park, PA 16801
3	Forrestal Campus Library Princeton University ATTN: Prof. M. Summerfield Dr. L. Caveny Tech Lib P.O. Box 710 Princeton, NJ 08540
2	Purdue University School of Mechanical Engrg ATTN: Prof. J. Osborn Prof. S. N. B. Murthy TSPC Chaffee Hall West Lafayette, IN 47906
1	Rutgers State University Dept of Mechanical and Aerospace Engineering ATTN: Prof. S. Temkin University Heights Campus New Brunswick, NJ 08903
1	Southwest Research Institute Fire Research Section ATTN: W. H. McLain P.O. Drawer 28510 San Antonio, TX 78228
1	Stanford Research Institute Propulsion Sciences Division ATTN: Tech Lib 333 Ravenswood Avenue Menlo Park, CA 94024
1	Stevens Institute of Technology Davidson Laboratory ATTN: Prof. R. McAlevy, III Hoboken, NJ 07030

DISTRIBUTION LIST

No. of Copies	Organization
1	University of California, San Diego AMES Department ATTN: Prof. F. Williams P.O. Box 109 La Jolla, CA 92037
1	University of Denver Denver Research Institute ATTN: Tech Lib P.O. Box 10127 Denver, CO 80210
1	University of Illinois Dept of Aeronautical Engrg ATTN: Prof. H. Krier Transportation Bldg, Rm 105 Urbana, IL 61801
1	University of Minnesota Dept of Mechanical Engrg ATTN: Prof. E. Fletcher Minneapolis, MN 55455
2	University of Utah Dept of Chemical Engrg ATTN: Prof. A. Baer Prof. A. Flandro Salt Lake City, UT 84112
1	Washington State University Dept of Mechanical Engrg ATTN: Prof. C. T. Crowe Pullman, WA 99163

No. of Copies	Organization
	Aberdeen Proving Ground
	Marine Corps LnO Dir, USAMSAA